ALI HAFEDH MAHMOOD ALKARKHI

ATILIM UNIVERSITY 2021

INVESTIGATION ON THE MECHANICAL BEHAVIOUR OF POLYMER CONCRETE FILLED ALUMINUM TUBES

THE GRADUATE SCHOOL OF NATURAL AND APPLIED SCIENCES
OF
ATILIM UNIVERSITY

ALI HAFEDH MAHMOOD ALKARKHI

A MASTER OF SCIENCE THESIS
IN
THE DEPARTMENT OF CIVIL ENGINEERING

MAY 2021

INVESTIGATION ON THE MECHANICAL BEHAVIOUR OF POLYMER CONCRETE FILLED ALUMINUM TUBES

A THESIS SUBMITTED TO
THE GRADUATE SCHOOL OF NATURAL AND APPLIED SCIENCES
OF
ATILIM UNIVERSITY

BY

ALI HAFEDH MAHMOOD ALKARKHI

IN PARTIAL FULFILLMENT OF THE REQUIREMENTS
FOR
THE DEGREE OF MASTER OF SCIENCE
IN
THE DEPARTMENT OF CIVIL ENGINEERING

MAY 2021

Approval of the Graduate School of Natural and Applied Sciences, Atilim University.

_____

Prof. Dr. Ender KESKİNKILIÇ
Director

I certify that this thesis satisfies all the requirements as a thesis for the degree of **Master of Science in Civil Engineering Department, Atilim University**.

_____

Prof. Dr. Hasan Umur AKAY
Head of Department

This is to certify that we have read the thesis INVESTIGATION ON THE MECHANICAL BEHAVIOUR OF POLYMER CONCRETE FILLED ALUMINUM TUBES submitted by ALI HAFEDH MAHMOOD ALKARKHI and that in our opinion it is fully adequate, in scope and quality, as a thesis for the degree of Master of Science.

_____	_____
Asst. Prof. Dr. Cemal Merih Şengönül Co-Supervisor	Prof. Dr. Tolga Akış Supervisor

Examining Committee Members:

Prof. Dr. Ahmet Hakan Argeşo
Manufacturing Eng. Department, Atilim University _____

Prof.Dr. Tolga Akış
Civil Eng. Department, Atilim University _____

Doç. Dr. Caner Şimşir
Metallurgical and Materials Eng. Department, METU _____

Date: *May 6, 2021*

I hereby declare that all information in this document has been obtained and presented in accordance with academic rules and ethical conduct. I also declare that, as required by these rules and conduct, I have fully cited and referenced all material and results that are not original to this work.

Name, Last Name: Ali Hafedh Mahmood Alkarkhi

Signature:

ABSTRACT

INVESTIGATION ON THE MECHANICAL BEHAVIOUR OF POLYMER CONCRETE FILLED ALUMINUM TUBES

Alkarkhi, Ali Hafedh Mahmood

M.S., Department of Civil Engineering

Supervisor: Prof. Dr. Tolga Akış

Co-Supervisor: Asst. Prof. Dr. Cemal Merih Şengönül

May 2021, 80 pages

This research focuses on the mechanical behaviour and confinement effect of aluminum tubes on a novel polymer concrete (PC) composed of recycled waste foundry sand (WFS), epoxy resin, and rice husk ash (RHA). In addition, we explored the effect of carbon fiber reinforcement (CFRP) on the axial load carrying capacity of polymer concrete-filled aluminum tubes (PCFATs) and determined the main influencing factors of both confinements. Specimens having dimensions of length 120, 150, 180, 210 mm, diameter 40, 50, 60, 70 mm, and thickness 2, 3, and 4 mm were prepared. We tested three specimens for each geometry under compression for three sets of experiments, where hollow circular aluminum tube (HCAT), PCFAT, and carbon fiber reinforced PCFAT (CFPCFAT) specimens were used. We employed two confinement models separately for the PCFAT and CFPCFAT. It is found that both diameter and thickness influence the composite tube's axial load carrying capacity, and the thickness plays a significant role, especially in failure modes. The experimental results also showed the enhancement in the load-carrying capacity when CFRP was used. Moreover, test results show good agreement with the confinement model calculations for PCFAT specimens. On the other hand, the model for the CFPCFATs gives conservative results compared to the experimental ones.

Keywords: PCFAT, CFPCFAT, CFRP, Polymer concrete, Confinement, Waste foundry sand.

ÖZ

POLİMER BETON DOLGULU ALÜMİNYUM TÜPLERİN MEKANİK DAVRANIŞININ ARAŞTIRILMASI

Alkarkhi, Ali Hafedh Mahmood

Yüksek Lisans, İnşaat Mühendisliği Bölümü

Tez Yöneticisi : Prof. Dr. Tolga Akış

Ortak Tez Yöneticisi : Dr. Öğr. Ü. Cemal Merih Şengönül

Mayıs 2020, 80 sayfa

Bu araştırmada atık döküm kumu, epoksi ve pirinç çeltiği külünden üretilen yeni bir polimer betonla doldurulmuş alüminyum tüplerin mekanik davranışı ve sargılama etkileri incelenmiştir. Ayrıca, karbon fiberle güçlendirmenin polimer beton dolgulu alüminyum tüplerin eksenel yük kapasitesine etkisi ve her iki sargılama yönteminin temel faktörleri araştırılmıştır. Test numuneleri, 120, 150, 180 mm uzunluklarında, 40, 50, 60 ve 70 mm çaplarında veya 2, 3 ve 4 mm kalınlıklarında hazırlanmışlardır. Boş alüminyum tüp, polimer beton dolgulu alüminyum tüp ve karbon fiberle güçlendirilmiş polimer beton dolgulu alüminyum tüpler olmak üzere üç farklı gruba ayrılan deneylerde her geometri için 3 numune kullanılmıştır. Polimer beton dolgulu alüminyum tüpler ve karbon fiberle güçlendirilmiş polimer beton dolgulu alüminyum tüpler iki farklı sargılama modeli kullanılarak incelenmiştir. Tüp çapı ve kalınlığın kompozit tüplerin eksenel yük taşıma kapasitesini etkilediği görülmüştür. Tüp kalınlığının özellikle göçme biçimi üzerinde önemli bir etkiye sahip olduğu gözlenmiştir. Deney sonuçları ayrıca karbon fiberle güçlendirmenin yük taşıma kapasitesini önemli oranda artırdığını göstermiştir. Bunların yanı sıra polimer beton dolgulu alüminyum tüpler için kullanılan sargılama modelinin deneysel sonuçlarla uyum içerisinde olduğu belirlenmiştir. Karbon fiberle güçlendirilmiş polimer beton

dolgulu alüminyum tüpler için kullanılan sargılama modeli ise deney sonuçları göz önünde bulundurulduğunda oldukça güvenli tarafta kalmıştır.

Anahtar Kelimeler: Polimer beton dolgulu alüminyum tüp, Karbon fiberle güçlendirilmiş polimer beton dolgulu alüminyum tüp, Karbon fiberle güçlendirilmiş polimer, Polimer beton, Sargılama, Atık döküm kumu.

To my family

ACKNOWLEDGMENTS

The author sincerely expresses his deepest gratitude to the God of science. I hope He blesses this work as an ongoing charity and a beneficial knowledge for Humanity to improve the construction field in the future.

First and foremost, the author would like to express his thanks to his supervisor Prof. Dr. Tolga Akış, Department of Civil Engineering, Atilim University. He has always been a tremendous mentor. His enthusiasm towards the advanced analysis of composite materials, patience, knowledge, and constructive advice has been the key to successfully complete this thesis.

The author also wishes to express his deepest gratitude to his co-supervisor, Asst. Prof. Dr. Cemal Merih Şengönül, Department of Manufacturing Engineering, Atilim University, for his invaluable suggestions, motivation, and affectionate encouragement, which helped accomplish this study.

The author also takes the opportunity to pay his heartfelt thanks to staff members of Civil Engineering Laboratory Mr. Engin Alp and Mr. Dogan Tok, for their consistent support and painstaking contributions to the experimental work.

The author also would like to thank Mr. Bülent Aydoğan and Metal Forming Center of Excellence of Atilim University members for their help during laboratory work.

The author also would like to thank Duratek for providing the epoxy as donation. He is grateful to Mehmet Fikret Yıldırım from Ministry of Agriculture and Forestry-Soil, Fertilizer and Water Recourse Central Research Institute for providing the rice husk. He expresses his gratitude to Kemal Derman from Derman Döküm for providing waste foundry sand.

The author also appreciatively remembers his friends and well-wishers' assistance and encouragement and everyone related to carry out and complete this study.

Finally, the author wishes to express his deep gratitude to his father (Eng. Hafedh Alkarkhi), mother (M. Maryam Imran), and his siblings (Zain Alabideen, Mustafa & Anas) for believing in him, their constant support, encouragement, and sacrifice throughout the research work.

TABLE OF CONTENTS

ABSTRACT ..... **iii**

ÖZ ..... **v**

ACKNOWLEDGMENTS ..... **viii**

TABLE OF CONTENTS ..... **x**

LIST OF TABLES ..... **xii**

LIST OF FIGURES ..... **xiv**

LIST OF ABBREVIATIONS ..... **xviii**

LIST OF SYMBOLS ..... **xix**

CHAPTER

1. **INTRODUCTION** **1**

    1.1 Background 1

    1.2 Research scope and objectives 4

    1.3 Thesis outline 5

2. **LITERATURE REVIEW** **6**

3. **MATERIALS AND METHODOLOGY** **11**

    3.1 Introduction 11

    3.2 Materials 11

        3.2.1 Polymer concrete (PC) 11

        3.2.2 Aluminum tubes 17

        3.2.3 Carbon fiber 18

    3.3 Mechanical tests 20

        3.3.1 Aluminum coupon test 20

3.3.2 Compressive strength test 23
3.3.3 Specimen preparation 24
4. **RESULTS AND DISCUSSIONS 32**
4.1 Introduction 32
4.2 Aluminum coupon test results 32
4.3 Compressive strength test results 34
4.3.1 Compression test results of HCAT specimens 34
4.3.2 Compression test results of PCFAT specimens 37
4.3.3 Compression test results of CFPCFAT specimens 39
4.3.4 Stress-strain diagrams 43
4.3.5 Failure modes 55
4.3.6 Axial stiffness 58
4.3.7 Analytical models for predicting the load bearing capacity 61
CHAPTER 5 74
5. **CONCLUSION 74**
5.1 Conclusions 74
5.2 Future studies 75
REFERENCES 76

LIST OF TABLES

TABLES

Table 3.1 PC mixture proportions used in the study [11] 12

Table 3.2 Average mechanical properties of PC used in the study [11] 12

Table 3.3 Duratek AV 75 epoxy properties 14

Table 3.4 Chemical composition of WFS [11] 16

Table 3.5 Chemical composition of RHA [11] 16

Table 3.6 Chemical composition of 6082 T6 aluminum tubes 18

Table 3.7 Some properties of SikaWrap-230 C carbon fiber 19

Table 3.8 Some properties of SikaWrap-230 C epoxy 20

Table 3.9 Dimensions of the aluminum coupon test specimens 22

Table 3.10 Dimensions of HCAT specimens 26

Table 3.11 Dimensions of PCFAT specimens 28

Table 3.12 Dimensions of CFPCFAT specimens 31

Table 4.1 Coupon test results 33

Table 4.2 Axial load capacity of HCAT specimens 35

Table 4.3 Axial load capacity of PCFAT specimens 38

Table 4.4 Axial load capacity of CFPCFAT specimens 40

Table 4.5 Capacity increase of CFPCAT specimens 42

Table 4.6 Axial stuffiness of PCFAT specimens 59

Table 4.7 Axial stuffiness of CFPCFAT specimens 60

Table 4.8 Experimental variables and test results 63

Table 4.9 Calculated parameters and test results of PCFATs..... 67

Table 4.10 Calculated parameters and test results of CFPCFAT 72

LIST OF FIGURES

FIGURES

Figure 1.1 CFST used in bridges [4] 2

Figure 1.2 (a) Schematic view of CFST composite girder, and (b) Construction example [5] 3

Figure 1.3 (a) The application of PC with epoxy as a cover, and (b) The difference between repaired and unrepaired pavements [9] 4

Figure 1.4 (a) Schematic of PC railroad crossing system, (b) Installed PC railroad crossing system [10] 4

Figure 3.1 Duratek AV 75/A epoxy 13

Figure 3.2 Waste foundry sand 14

Figure 3.3 Drying oven (Elektro-Mag M6040P) 15

Figure 3.4 Granular gradation of WFS [11] 15

Figure 3.5 PLF 110- 130- Protherm furnaces oven 17

Figure 3.6 (a) Rice husk, and (b) Rice husk ash 17

Figure 3.7 (a) SikaWrap-230 C carbon fiber, and (b) SikaWrap-230 C epoxy 20

Figure 3.8 Coupon test specimen dimensions 21

Figure 3.9 Aluminum coupon test specimens 21

Figure 3.10 ZWICK ROELL Z300E testing machine 22

Figure 3.11 ALFA B-001 PC testing machine 23

Figure 3.12 Test setup 24

Figure 3.13 Specimens cut using KAR METAL 300 ODG 24

Figure 3.14 OSTİM MAKİNA SN 50 turning machine 25

Figure 3.15 HCAT specimens 25

Figure 3.16 PCFAT specimen..... 27

Figure 3.17 Preperation of (CFPCFAT) specimens..... 29

Figure 3.18 CFPCFAT specimens 30

Figure 4.1 True stress-strain curves for the aluminum coupon test..... 33

Figure 4.2 Mean ultimate lad capacity of HCAT Specimens 36

Figure 4.3 Load-displacement curves for HCAT120 specimens (D = 40 mm)..... 37

Figure 4.4 Load-displacement curves for HCAT180 specimens (D = 60 mm)..... 37

Figure 4.5 Mean ultimate stresses of PCFAT specimens 39

Figure 4.6 Mean ultimate stresses of CFPCFAT specimens 41

Figure 4.7 Stress-strain curves of (a) polymer concrete filled aluminum tube (PCFAT) and (b) carbon fiber wrapped PCFAT specimens having 40 mm diameter and 2 mm thickness..... 43

Figure 4.8 Stress-strain curves of (a) polymer concrete filled aluminum tube (PCFAT) and (b) carbon fiber wrapped PCFAT specimens having 40 mm diameter and 3 mm thickness..... 44

Figure 4.9 Stress-strain curves of (a) polymer concrete filled aluminum tube (PCFAT) and (b) carbon fiber wrapped PCFAT specimens having 40 mm diameter and 4 mm thickness..... 45

Figure 4.10 Stress-strain curves of (a) polymer concrete filled aluminum tube (PCFAT) and (b) carbon fiber wrapped PCFAT specimens having 50 mm diameter and 2 mm thickness..... 46

Figure 4.11 Stress-strain curves of (a) polymer concrete filled aluminum tube (PCFAT) and (b) carbon fiber wrapped PCFAT specimens having 50 mm diameter and 3 mm thickness..... 47

Figure 4.12 Stress-strain curves of (a) polymer concrete filled aluminum tube (PCFAT) and (b) carbon fiber wrapped PCFAT specimens having 50 mm diameter and 4 mm thickness..... 48

Figure 4.13 Stress-strain curves of (a) polymer concrete filled aluminum tube (PCFAT) and (b) carbon fiber wrapped PCFAT specimens having 60 mm diameter and 2 mm thickness 49

Figure 4.14 Stress-strain curves of (a) polymer concrete filled aluminum tube (PCFAT) and (b) carbon fiber wrapped PCFAT specimens having 60 mm diameter and 3 mm thickness 50

Figure 4.15 Stress-strain curves of (a) polymer concrete filled aluminum tube (PCFAT) and (b) carbon fiber wrapped PCFAT specimens having 60 mm diameter and 4 mm thickness 51

Figure 4.16 Stress-strain curves of (a) polymer concrete filled aluminum tube (PCFAT) and (b) carbon fiber wrapped PCFAT specimens having 70 mm diameter and 2 mm thickness 52

Figure 4.17 Stress-strain curves of (a) polymer concrete filled aluminum tube (PCFAT) and (b) carbon fiber wrapped PCFAT specimens having 70 mm diameter and 3 mm thickness 53

Figure 4.18 Stress-strain curves of (a) polymer concrete filled aluminum tube (PCFAT) and (b) carbon fiber wrapped PCFAT specimens having 70 mm diameter and 4 mm thickness 54

Figure 4.19 Failure mode of HCAT-150 specimens (D=50 mm) with (a) 4 mm (b) 3 mm (c) 2 mm thickness 55

Figure 4.20 Failure mode of HCAT-180-2-1 specimen (D=60 mm) 56

Figure 4.21 Failure mode of PCFAT-120 specimens (D=40 mm) with (a) 4 mm (b) 3 mm (c) 2 mm thickness 56

Figure 4.22 Failure mode of CFPCAT -150 specimens (D=50 mm) with (a) 2 mm (b) 3 mm (c) 4 mm thickness 57

Figure 4.23 Axial stuffiness of PCFAT specimens 58

Figure 4.24 Axial stuffiness of CFPCFAT specimens 61

Figure 4.25 0.2% offset yield strength of the HCAT120-2-1 specimen 62

Figure 4.26 Experimental axial compressive load capacities of polymer concrete-filled aluminum tubes 66

Figure 4.27 Comparisons between experimental and calculated values of PCFAT .. 68

Figure 4.28 Increase index of capacity 69

Figure 4.29 Increase in capacity versus ξ_{frp}/ξ_{al} 70

Figure 4.30 Comparison of the experimental and calculated results of CFPCFAT .. 71

LIST OF ABBREVIATIONS

AA	Aluminum Alloy
ACI	American Concrete Institution
ASTM	American Society for Testing and Materials
CFAT	Concrete Filled Aluminum Tube
CFPCFAT	Carbon Fiber Reinforced Polymer Concrete Filled Aluminum Tube
CFRP	Carbon Fiber Reinforced Polymer
CFSST	Concrete Filled Stainless Steel Tube
CFST	Concrete Filled Steel Tube
HCAT	Hollow Circular Aluminum Tube
ISO	International Organization for Standardization
PC	Polymer Concrete
PCFAT	Polymer Concrete Filled Aluminum Tube
RHA	Rice Husk Ash
SHS	Steel Hollow Sections
WFS	Waste Foundry Sand

LIST OF SYMBOLS

N_O	:	Nominal squash load
N_{PCFAT}	:	Load capacity of the PCFAT under axial compression
N_{SO}	:	Axial yield strength of aluminum tube
N_u	:	Theoretical ultimate strength of aluminum tube
f_c'	:	Compressive strength of filled polymer concrete
f_{cf}	:	Tensile strength of CFRP sheet
f_{ck}	:	Characteristic strength of concrete
f_u	:	Tensile strength of aluminum
f_y	:	Yield strength of aluminum
α_u	:	Material coefficients
β_{uc}	:	Material coefficients
γ_u	:	Strength reduction factor
ξ_{al}	:	Confinement factor of aluminum tube
ξ_{frp}	:	Confinement factor of CFRP wrap
$\sigma_{0.2}$	:	0.2% proof stress of aluminum
σ_{ccB}	:	Strength of confined polymer concrete
σ_r	:	Lateral pressure
σ_{scy}	:	Compressive yield stress
σ_{sy}	:	Mean tensile yield stress of aluminum tube
σ_{sz}	:	Axial stress
$\sigma_{s\theta}$	:	Hoop stress
A_{al}	:	Cross-sectional area of aluminum
A_{PC}	:	Cross-sectional area of concrete
N_{exp}	:	Experimental ultimate axial load
K	:	Axial stiffness
N	:	Axial load
P	:	Applied load

k	:	Confinement coefficient
δ	:	Axial shortening
η_{cap}	:	Increase index of capacity
λ	:	Augmentation factor
σ	:	Compressive strength

CHAPTER 1

INTRODUCTION

1.1 Background

The term concrete traditionally refers to the composition of cement, aggregate, and water. Historically, the first concrete structure to-date goes back to 6500 BC in Syria and Jordan. In 3000 BC, the ancient Egyptians used mortar (cement and water), an abstract of concrete, as a binding agent for the construction of the Great Pyramids of Giza. On the other hand, the Romans were the first to use this highly resistant material widely. They produced the high-resistance concrete by mixing cement with volcanic ash and seawater, then they formed columns, piles, bridges, and floorings by pouring the mixture into wood panels. The first great leap in the concrete technology came in 1759 when John Smeaton discovered a cutting-edge method by utilizing burnt and pulverized limestone to produce hydraulic lime cement [1]. This type of cement was used in the rebuilding of the Eddystone Lighthouse in Cornwall, England. Another significant milestone in the evolution of cement happened in 1824 when Joseph Aspdin invented Portland cement by burning finely ground chalk and clay until the carbon dioxide was removed [2]. Since then, there has not been a noticeable advancement to conventional cement.

Concrete is a highly functional material, yet it has some setbacks. For example, it has high resistance under compression, but its flexural strength is about 10 to 20 percent of its compressive strength. Also, concrete fails easily under tensile and bending stresses with little to no deformation (brittle). Joseph Monier introduced in the mid-19th century reinforced concrete (RC) which is fortified with steel bars that has high tensile strength and ductility [3]. Due to its fire and weather resistance, and high compressive strength, RC has been widely used in the construction of high-rise buildings, roads, dams, and stadiums since the 19^{th} century.

One disadvantage of RC structures is their heavy weight. One column of RC concrete can easily weigh several tons, which can put unwarranted stresses on the superstructure and substructure. In addition, once bending stresses are applied, one part of the concrete is exposed to tensile, while the other part is subjected to compressive stresses. Hence, the concrete casting ends up with plastic shrinkage cracks while the embedded steel bars are fully intact. Since steel has drastically high tensile strength, it may be more practical to confine the concrete inside the steel tubes instead of embedding them inside the concrete. Consequently, concrete-filled steel tubes (CFST) have become more significant in the construction of high-rise buildings and other facilities where any margin of error can cause catastrophic failures. Another benefit of CFST is that it reduces the cross-sectional area of the structural member considerably, which is ideal for the construction of bridge footings where space is scarce. CFST also eliminates the messy process of concrete casting since the tubes themselves serve as casting molds. Such an approach also cuts back labor costs. The placement of steel around the perimeter of the structural elements provides the highest flexural capacity and moment of inertia for these sections. Some examples of CFST applications are shown in Figs. 1.1 and 1.2, respectively.

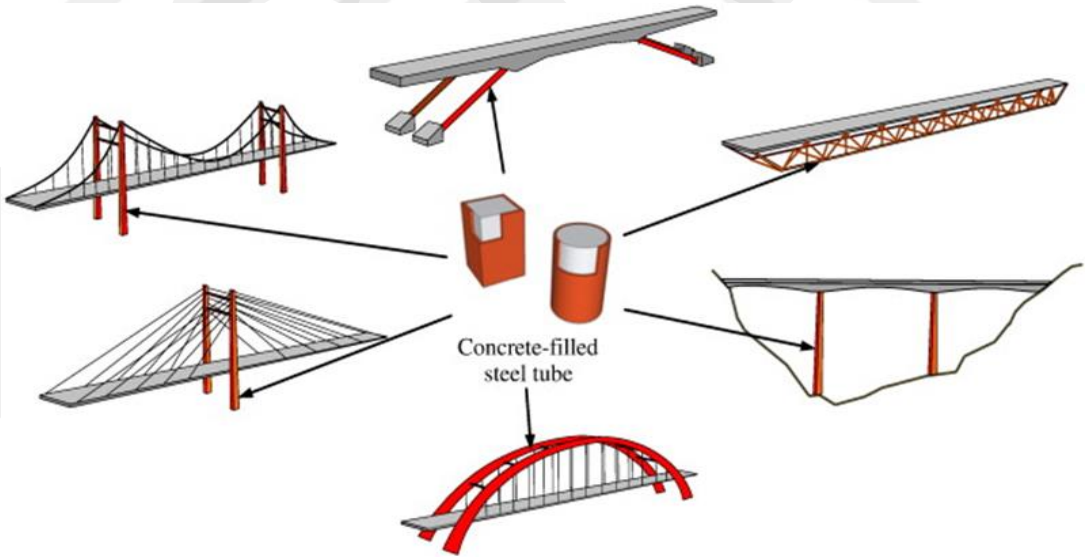

Figure 1.1 CFST used in bridges [4]

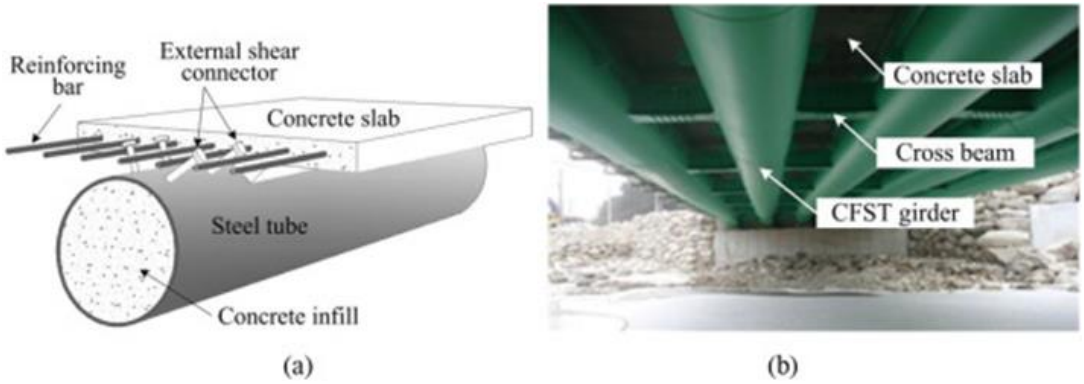

Figure 1.2 (a) Schematic view of CFST composite girder, and (b) Construction example [5]

However, some studies have shown that the ends of the CFSTs are often prone to plastic buckling (elephant leg), especially in seismic earthquake regions. As a remedy, application of fiber-reinforced composite materials, such as carbon fiber reinforced polymers (CFRP) as confinement on the surface of the CFSTs can delay or limit the local buckling as well as enhance the other mechanical properties of the material [6].

On the other hand, steel tubes can be quite heavy and can corrode in an unfavorable way over time. Its light weight and high resistance to corrosion render aluminum a substitute for steel tubes. Currently, aluminum confinements are widely used in high-rise buildings like the Bank of China and the Empire State Building, where the heavy steel confinements were replaced by aluminum tubes. Besides, their easy maintenance and good appearance make them a favorable alternative to steel. According to recent studies, additional CFRP confinement could increase the ultimate strength as well as delay the local buckling of the CFATs [7].

To overcome the heavy weight problem of RC, CFST, and CFAT, fiber-reinforced concrete (FRC) was introduced in 1970's. FRC weighs considerably less than RC without compromising the tensile strength of the structure too much. The next significant step of the evolution of concrete comes during the cold war with the introduction of polymer concrete (PC).

PC is a material made by entirely substituting the cement hydrate binders of traditional cement concrete with liquid thermoset polymer resins. In that sense, it is a polymer composite material. Thermosetting resins in liquid form are left to curing process at

ambient or room temperatures to attain a hard polymer composite structure. Polymer resin is highly superior to conventional cement in terms of impact resistance, compressive strength, durability, anti-freezing and thawing, low permeability, and resistance to chemical attacks and erosion. Additionally, one of the essential PC applications is patching and repairing concrete structural elements [8]. PC is a supreme material with a high initial cost, but since it needs little to no maintenance, it is an excellent long-term investment. Some of the PC applications are shown in Figs. 1.3, and 1.4.

Figure 1.3 (a) The application of PC with epoxy as a cover, and (b) The difference between repaired and unrepaired pavements [9]

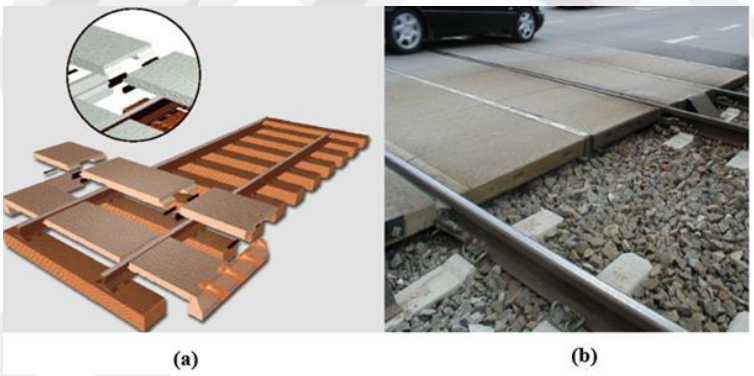

Figure 1.4 (a) Schematic of PC railroad crossing system, (b) Installed PC railroad crossing system [10]

1.2 Research scope and objectives

This study's scope is to carry out an experimental and analytical investigation on the mechanical behaviour of polymer concrete-filled cylindrical aluminum tubes (PCFAT) under compressive loads using a novel polymer concrete developed by Alganad et al. at Atilim University [11]. Experimental results are used to evaluate the

confinement performance of lone aluminum tubes (PCFAT) and carbon fiber reinforced aluminum tubes (CFPCAT) for PC under compression. Furthermore, the load capacity and axial stiffness of the specimens with the failure modes according to various slenderness ratios (length (L) / wall thickness (t), and diameter (D) / wall thickness (t)) has been investigated. Finally, two confinement models based on the axial load capacity of PCFAT and CFPCFAT are utilized comparatively.

1.3 Thesis outline

This thesis consists of five chapters. In the first chapter, the background, scope and objectives of this study are introduced. It is followed by a literature review given in the second chapter. In the third chapter, materials used, experimental design, specimen preparation, and the test methods are described. In the fourth chapter, the results of the experiments and their implications are discussed. In addition, the confinement models used to predict the capacity of the composite assemblies are presented in this chapter. Finally, the conclusions and recommendations for future work are given in the fifth chapter.

CHAPTER 2

LITERATURE REVIEW

This chapter presents a literature review of some of studies on concrete filled circular and rectangular tubes explored under different types of loads with different confinement conditions.

Huang et al. [12] proposed a stiffening scheme that could improve the mechanical properties of concrete-filled steel square tubes (CFST). It was based on the investigations of the axial load behaviour of CTSF columns. In the study, they tested the ductility, stiffness, and strength of 17 specimens to determine the effect of reinforcement, width-to-thickness ratios, and cross-sectional shapes. Axial stress distribution and its impact on ultimate strength was also investigated. Results obtained showed that their proposed stiffening scheme could increase the ductility and strength of CFST columns.

Giakoumelis and Lam [13] underlined how CFST with disparate concrete strength behaved under axial load. Fifteen specimens that had D/t ratio of about 22 and 31 and concrete strength of between 30 and 100 N/mm^2 were tested. They examined the confinement effect on concrete, the bond strength between the steel tube and the concrete, and the effect of tube thickness on the strength of the composite structure. The strength values were then compared with those predicted in American codes, Australian standards, and Eurocode 4. Experimental results show that the estimates of all the codes were lower compared to those obtained in their experiments.

Ellobody et al. [14] investigated the design and behaviour of axially loaded CFST circular stub columns. A wide array of concrete cube strength range was used. In their study, they developed a finite element (FE) model that was quite accurate. The results of the FE model were compared with results obtained from real-life experiments. The predicted results were then compared with European, Australian, and American

specifications. They showed that the design strength in all the above codes were not as accurate as the Australian and American specifications, which are quite conservative.

Gupta and colleagues [15] studied the behaviour of circular concentrically loaded CFSTs based on computational and experimental methods. Using 81 specimens, the effect of fly ash in concrete and the grade of the concrete, among other aspects, were investigated. Strength results of the CFST columns obtained by experiments were compared with those available in the literature. A nonlinear finite element model was also developed and used to identify the load carrying mechanism of the CFST columns. The studies showed that in both modes of failure, the load-carrying capacity tends to decrease with an increase amount of fly ash up to 20 percent by volume in the concrete composition.

CFST stub columns subjected to axial local compression were experimentally investigated by Han et al. [16]. A finite element model was also used to determine the composite columns' failure mechanisms. Results showed a good agreement with test results.

Oyawa et al. [17] attempted to overcome the limitations imposed by certain drawbacks of cement concrete which cannot be alleviated or moderated by the encasing steel tubes such as the high shrinkage amount, creep, brittle fracture, reactivity, and low tensile strength. The study was conducted using 4 inert polymer-based materials filled in to steel tubes as replacement for the ordinary concrete with a variation of slenderness ratio in the thickness and the diameter. According to the results, the epoxy polymer concrete filled steel stub columns have high ductility but a moderate strength.

Guo and Zhang investigated three different carbon fiber reinforced polymer (CFRP) confinement of the stub-filled concrete steel tubular columns (CFST) [6]. The compressive strength and the physical properties of the composite columns having circular CFRP, inner circular CFRP, and outer square CFRP were studied. The axial bearing capacities of these three CFRP-confined CFST columns were calculated based on the elastoplastic limit equilibrium theory. They found that the outer circular CFRP had the best confinement effect and the outer square CFRP performed better than inner circular CFRP.

Tang et al. [18] explored the behaviour of fiber reinforced polymer (FRP) confined concrete filled stainless steel tube (CFSST) stub columns under axial loading. The test conducted using six CFSST stub columns and 18 FRP confined CFSST stub columns. The results showed that the load bearing capacity was increased around 71.35%, meanwhile energy absorption capacity was enhanced considerably. In addition, it was found that the load bearing capacity increased almost linearly with the increase in the number of CFRP wrapping layers.

Zhou and Young [19] studied concrete-filled aluminum (CFA) stub columns. Several tests were performed to investigate the effect of concrete strength, thickness, and aluminum tube confinement on the strength of the CFA stub columns with rectangular and square sections. The strength values were compared with Australian/New Zealand and American specifications. It was found that the experimental results do not agree well with the specified design strengths.

In a similar study, Zhou and Young [20] studied the CFA circular hollow section (CHS) stub columns. The effect of the geometric dimension of the aluminum CHS on concrete filled columns was investigated. Cylinders with various strength values were used to determine the structural performance of the stub columns under uniform axial compression. The authors presented the failure modes, the load axial shortening and strain relationship, and the strength of the CHS stub columns. The test results were also compared with American and Australian/New Zealand codes. Both the American and Australian/New Zealand specifications were found to be conservative.

In another work, by the same authors [21], results of a numerical investigation and a design procedure for CFA CHS columns were presented. They also developed a non-linear FE model and used it in verifying the results obtained in the experiments. The effect of material properties and cross-sectional geometry were also investigated. Over 190 numerical data were presented by these authors. The experimental and FE model results were compared with common specifications for concrete and aluminum structures. In addition, Zhou and Young [21] presented column design equations which are based on collective action of concrete infill and the aluminum CHS tube. Results show that these design equations could accurately predict the strength values of the CFA and CHS columns.

Nayak et al. [22] studied the effect of length to depth ratio (L/D) and depth to thickness ratio (D/t) on the self-compacting concrete (SCC) filled composite aluminum tubes under axial compression tests. The results obtained in their study showed that using SCC with aluminum tubes is an excellent choice as it enables the structure to withstand considerable amounts of load.

Idan [23] developed a nonlinear FE model to identify the behaviour of aluminum and concrete more precisely and to reconcile the confining effects of aluminum tubes on the concrete core. The model was developed using ANSYS. The accuracy of the model was validated by experimental results. The model was then used to underline the sway of the high strength concrete on the concrete filled aluminum column when subjected to axial load. Results show that the specimens that had high strength concrete experienced an increase in ultimate load capacity. However, these specimens showed a decrease in ductility.

Zhou and Young [24] studied numerically and experimentally the double skin aluminum hollow section stub columns. Tests were conducted to explore the effect of the geometric dimensions of the aluminum circular hollow sections on the concrete strength and deformation of the columns. The authors further developed a FE model, the results of which were verified by experimental data. The tests were compared with American specifications for concrete and aluminum structures. Further, design equations were also proposed in their study. Accordingly, the design equations were found to predict the ultimate strength of the columns accurately.

Talebi et al. [25] developed a nonlinear 3D FE model to study the seismic damage effects on concrete-filled tube columns. Structural, thermal, and cyclic loading tests were conducted in their study. The finite element model was compared with available fire and cyclic loading tests. The fire-resistance time and the axial deformation history were also presented in their study.

Rexin et al. [26] explored the strengthening mechanism of basalt fiber reinforced plastics on the concrete-filled rectangular tubular columns under compression. Ten columns were casted, and one of them was used as control. The comparative results show that columns with narrow spacing of basalt strips had better performance relative to those with wide spacing basalt strips.

Wang et al. [27] presented FE models based on nonlinearities of aluminum and concrete on CFAT stub columns subjected to axial compression. The failure modes, the load versus axial strain relationship, and the ultimate strength predictions were compared with experimental results. They also proposed equations for analytical calculation of the ultimate strength of these composite structures. Further, they also investigated the applicability of existing design methods for concrete-filled aluminum and steel tubular columns.

Patel et al. [28] investigated the design procedures of the circular high strength concrete-filled aluminum tubular (CFAT) columns loaded concentrically and determined the mechanical behaviour of them. They also proposed a novel concrete confinement model which can compute the lateral pressure. They also proposed design equations that can quantify the ultimate axial strength of the columns based on the Liang-Fragomeni's expression. Results indicate that both the design equations and the numerical modeling produced accurate outcomes.

Zhu et al. [7] studied the strengthening mechanism of conventional concrete-filled aluminum alloy tube (CFAT) beams having rectangular and square hollow sections (RHS and SHS) by using a layer of carbon fiber reinforcement polymer (CFRP). Thirty rectangular and square CFAT beams were strengthened with CFRP, while ten were used as control. Results show that the CFRP enhanced the flexural stiffness of the beams, meanwhile decreased the ductility of the beams. Results also showed that the four-sided bounded CFRP scheme performed better than the bottom flag-bonded CFRP in increasing the ultimate strength of the beams. They also proposed a novel design approach for appraising initial and final yield flexural stiffness of beam strengthened by CFRP. According to their final conclusion, carbon-fiber reinforced polymer reinforcement remarkably increased the ultimate strength of CFAT beams and could delay outward local buckling.

CHAPTER 3

MATERIALS AND METHODOLOGY

3.1 Introduction

An experimental program was conducted to determine the behaviour of polymer concrete-filled aluminum tubes (PCFAT) under axial compression. An extensive study was performed using 108 specimens divided into three groups, hollow circular aluminum tubes (HCAT), polymer concrete-filled aluminum tubes (PCFAT), and carbon fiber reinforced polymer concrete filled aluminum tubes (CFPCFAT), with a variety of lengths, diameters, and thicknesses. The length-to-diameter ratio was kept constant for all columns. All tests were carried out at the Civil Engineering Laboratory of Atilim University. In this chapter, properties of materials used in composite tubes, sample preparation, geometric dimensions, and information on the methodology are given.

3.2 Materials

3.2.1 Polymer concrete (PC)

Polymer concrete (PC) refers to concrete in which a liquid resin is used as a binder instead of using cement and water. The aggregate used in general is the same as ordinary concrete. Commonly used resins include unsaturated polyester resin, phenolic resin, and epoxy resin. On the other hand, cement can be added to the PC as a filler because there is no chemical reaction between the polymer and the cement [29]. Due to the use of PC, many characteristics might change by selecting different formulations. PC has high rigidity, corrosion resistance, and high compressive, tensile, and flexural strength. Furthermore, PC has high ductility, tenacity, impermeability, and antifreeze resistance. It can be used as a high-performance construction material in special projects, such as constructing pipes, piles, columns, floor tiles, marine structures, sidewalks, and bridge decks in corrosive media and parts with high

requirements for impact resistance, and in water conservation projects. It can also be used to fix structural surfaces and defects on-site to improve performance [30]. Nonetheless, in terms of economic benefits, the cost of PC is higher than the cost of regular cement concrete. Still, the former's price is often lower than the latter compared to unit strength and service life.

In the present study, a particular type of PC consisting of epoxy, waste foundry sand, and rice husk ash is used. It was developed by Alganad, and tested in 2020 [11]. Mixture ratios and the PC's mechanical properties used in this research are given in Tables 3.1 and 3.2, respectively.

Table 3.1 PC mixture proportions used in the study [11]

Epoxy	WFS	RHA
22.5%	67.5%	10%

Table 3.2 Average mechanical properties of PC used in the study [11]

Compressive strength	Splitting tensile strength	Flexural strength
51.88 MPa	12.51 MPa	21.74 MPa

3.2.1.1 Epoxy

Epoxy which is also called as synthetic resin, resin gum, etc., is an essential thermoplastic form and is widely used in adhesives, coatings, as well as other applications. Synthetic resins (epoxy/polyepoxide resin) are epoxy polymer thermosetting resins. Since the beginning of the 20th-century, investigations on epoxides have been done. It was commercially available in the mid-1940s as a coating material. Nowadays, epoxy resin is used in layers of composite materials for printed circuit boards, various electronic devices, integrated circuit packaging materials, reinforced plastic fiberglass products, water towers, yachts, etc. It is also widely used in coatings, adhesives, and structural reinforcement. For civil engineering, it can be combined with carbon fiber or glass fiber together to form a reinforcement material

with extremely high tensile strength having a wide range of applications. Chemically, by combining its fundamental components, hardening the epoxy is carried out, and the form of reaction significantly influences epoxy applications [31].

Epoxy is one of the most inspiring elements in the repair materials for Portland cement concrete (PCC) structural elements because of its high adhesiveness. Around 5 percent of total epoxy manufactures are producing it for adhesive purposes through statistical studies. Epoxy resins are manufactured in two forms (resin and hardener) for cold curing (curing at ambient temperature). Acrylates are usually better suited for epoxy adhesives among all modifiers [31].

The AV 75 epoxy supplied by Duratek was used for the production of the PC in this study. AV 75 consists of two components and cures after applying the hardener to the resin. It is shown in Fig. 3.1, and some of its properties are listed in Table 3.3.

Figure 3.1 Duratek AV 75/A epoxy

Table 3.3 Duratek AV 75 epoxy properties

Density	1.09 ± 0.05 g/cm^3
Viscosity (at room temperature)	1000 ± 200 mPa.s
Water absorption and permeability	> 0.1 kg/m^2 .h$^{0.5}$

3.2.1.2 Waste foundry sand

The wasted sands are the primary waste produced by the foundry industry. Due to the large volumes produced and the need to develop feasible practices that aim to accommodate them integrally, its management is considered as a big problem worldwide. Waste foundry sand (WFS) has historically been. It is used as a filling material for the situation of quarry cellars, brickyards, and lowlands, which means a risk of exposure to the underground water resource, considering the likely existence of metals, phenols, and polycyclic aromatic hydrocarbons, which are the process that adds. After studying its components, it was found that, despite being from waste, it is quality silica sand, and this has opened the door to many other studies that show promising results in the possibility of reuse as an alternative to fine aggregates in the construction industry and this solution encourage many countries and factories to get rid of the negative environmental and economic antiquities [32].

Figure 3.2 Waste foundry sand

The WFS used in this study is shown in Fig.3.2. It was provided by Derman Döküm Industries Ltd. Ankara, Turkey. It was oven-dried at 110 ± 5 ˚C for 24 hours, then cooled down to room temperature and stored there for another 24 hours before using in accordance with the ASTM D2974 standard [33], as sand can retain moisture. The oven used for the drying process was the elektro-mag M6040P, which is shown in Fig. 3.3. The granular gradation of the WFS and its chemical composition is given in Fig. 3.4 and Table 3.4, respectively, [11].

Figure 3.3 Drying oven (Elektro-Mag M6040P)

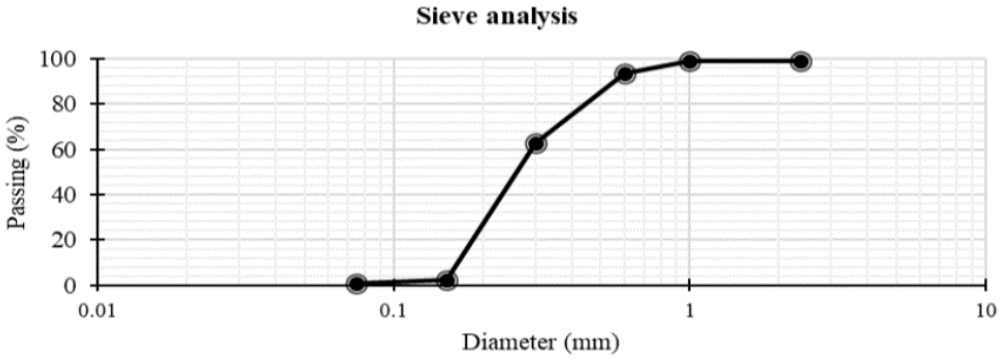

Figure 3.4 Granular gradation of WFS [11]

Table 3.4 Chemical composition of WFS [11]

Element	Si	Al	Fe	Ca	P	Ti	Mn	Mg	Cr
Weight %	98.27	0.44	0.39	0.35	0.10	0.09	0.04	0.01	0.01

3.2.1.3 Rice husk ash

Rice is known to be the world's most common crop. The world produces more than 600 million tons of rice per year, and the rice husks are typically useless after processing. Some European and American researchers investigated the rice husk ash (RHA) usage in the construction industry, and they discovered that RHA would minimize environmental pollution. The potential value of rice husk ash (RHA) as a building material was discovered a few years ago. RHA is rich in silica, an essential concrete component. It becomes stronger and has more resistant to abrasion when RHA is combined with concrete. It was also found that a replacement of RHA up to 30 percent in cement gives the same workability.

In this research, RHA was used as a PC filler similar to the Alganad et al. study [11]. The chemical composition of the RHA used is given in Table 3.5. Rice husk is typically converted to ash at temperatures between 500-700˚C [34]. In order to obtain RHA, the rice husk was burned at 600˚C in the PLF series 110-130-protherm furnaces, as shown in Fig. 3.5. It was then grinded and passed through sieve #200 with an opening diameter of around 75 μm. Both rice husk and rice husk ash are shown in Fig. 3.6.

Table 3.5 Chemical composition of RHA [11]

Element	Si	Al	Fe	Ca	P	Ti	Mn	Mg	S
Weight (%)	87.21	0.32	0.57	3.19	6.13	0.03	0.30	0.66	1.21

Figure 3.5 PLF 110- 130- Protherm furnaces oven

(a) **(b)**

Figure 3.6 (a) Rice husk, and (b) Rice husk ash

3.2.2 Aluminum tubes

Aluminum is one of the most common products in different industries in the world due to its adaptability and comparative advantages with other types of materials. With 8.13 percent of the total crust mass, it is the third most abundant element in the Earth's crust after oxygen and silicon. In terms of efficiency, it is three times lighter than steel and is characterized by high ductility in addition to the aesthetic shape that can be added to structures that rely on aluminum for cladding [35].

The hollow circular aluminum tubes (HCAT) used in the present study have four different outer diameters (D), specimen lengths (L), and three wall thicknesses (t). The tubes are cut from 3.0m long cold rolled circular 6082 T6 tubes provided by Setkoç Aluminyum Factory. The chemical composition of the aluminum tubes is given in Table 3.6.

Table 3.6 Chemical composition of 6082 T6 aluminum tubes

STANDART	Fe	Si	Mn	Cr	Ti	Cu	Mg	Zn	Each
Min		0.7	0.4				0.6		
Max	0.5	1.3	1	0.25	0.1	0.1	1.2	0.2	0.05

3.2.3 Carbon fiber

Carbon fibers and their composites are new technologies that have evolved with the development of the military industry. It is a product with high specific strength, relatively high modulus, high temperature, wear, fatigue, creep resistance, and electrical conductivity and transport. It can be used as a structural material for load transmission and as a functional material with excellent properties. As a result, it has developed rapidly in recent years. It has been widely used in many fields such as aviation, space, automotive, environmental engineering, chemical industry, transportation, construction, energy, electronics, and sports equipments.

In civil engineering and construction materials, the quantity of cement is the highest, but cement has limitations such as high brittleness and low tensile strength. In order to strengthen these weaknesses, carbon fiber reinforced composites with concrete or asphalt as the matrix is used. In civil engineering applications, as carbon fiber and aramid fiber have the characteristics of high strength, large module, low specific gravity, alkali corrosion resistance, and are harmless to humans and animals, their usage is increasing [36].

The composite material sheet of carbon fiber is a sheet consisting of bundles of carbon fiber that are aligned and bonded at room temperature by a thermoplastic resin (usually

epoxy resin). This type of plate is applied to the structure's reinforced section according to the design specifications in order to increase the impact strength modulus and tensile strength in repairing and strengthening the reinforced concrete structures. In some projects, such as strengthening the reinforced concrete bridge slabs damaged after the earthquake and reinforcing the oil platform walls, carbon fibers have made breakthroughs. Carbon fiber composite sheets provide the advantages of lightweight (specific gravity is 1/4 1/5 of iron), the tensile modulus is more than ten times higher than steel, excellent wear resistance, hand-holding and good workability. Additionally, in the repair and reinforcement of deteriorating reinforced concrete, the use of carbon fiber composite material may improve the structural endurance and strengthen the structures. In civil engineering, the application of carbon fibers is still a new technology. Recently, the use of carbon fibers has increased, and the price has decreased with the increase in production in the field of construction. At the same time, some studies showed that the price of the fiber-reinforced material is higher, the overall cost of material, cost of construction, and cost of use are relatively similar but, fiber-reinforced materials are stronger in terms of anti-corrosion and lightweight construction, and this leds to expanding in the application areas with high-performance fibers [37].

The unidirectional carbon fiber used in the present study is SikaWrap-230 C, and it has been provided by the Sika Factory in Turkey, as shown in Fig. 3.7. It has a mid-range strength designed for installation using the dry or wet application process. It has a three-component system, carbon fiber, epoxy, and hardening agent. Some of the carbon fiber characteristics are shown in Table 3.7 and the properties of the epoxy are listed in Table 3.8.

Table 3.7 Some properties of SikaWrap-230 C carbon fiber

Laminate nominal thickness	0.129 mm
Laminate nominal cross section	129 mm^2 per m width
Laminate modulus of elasticity in tension	3 500 N/mm^2
Laminate tensile strength	225 kN/mm^2
Laminate elongation at break in tension	1.59%

(a) **(b)**

Figure 3.7 (a) SikaWrap-230 C carbon fiber, and (b) SikaWrap-230 C epoxy

Table 3.8 Some properties of SikaWrap-230 C epoxy

Shear strength	> 12 N/mm^2
Expansion	< 0.1%
Workability	65 min. at 23 ˚C
Modulus of elasticity in compression	>2000 N/mm2
Coefficient of thermal expansion	<100*10^{-6}

3.3 Mechanical tests

In this part, the details of the mechanical tests on the materials and composite assemblies are presented.

3.3.1 Aluminum coupon test

Coupon samples taken from the aluminum tubes used in the tests are essential for two main reasons. Firstly, to obtain aluminum properties such as yield and fracture strengths used in the modelling studies and measurements is important. Secondly, it should verified that the 6082-T6 aluminum tubes have similar properties. Otherwise, new parameters should be considered when comparing the specimens.

The dimensions required for the coupon specimens depends on several factors, such as the test equipment available. Fig. 3.8 shows the dimensions of a sample of a steel coupon. For this test, the specimens are prepared from 6082-T6 aluminum rectangular tubes. The samples were extracted from the aluminum plate in the Civil Engineering Laboratory, as shown in Fig. 3.9. The test was done using (ZWICK ROELL Z300E) testing machine according to DIN EN 10002-1,04/1991 [38], ISO 10113,05/1991, and ISO 10275,02/1993 [39] standards. Fig 3.10 shows the testing machine. Since the temperature affects the aluminum's reaction with the test, the temperature ramp is taken as 10 °C/min, and the temperature after the end of the test is measured as 23 °C. The coupon sample's actual dimensions were manually measured using a vernier and are listed in Table 3.9.

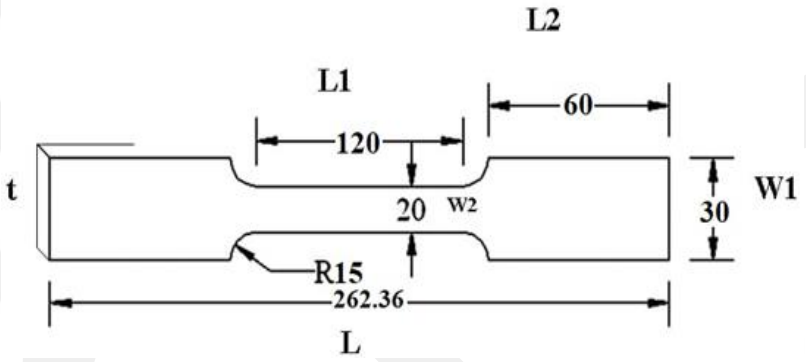

Figure 3.8 Coupon test specimen dimensions

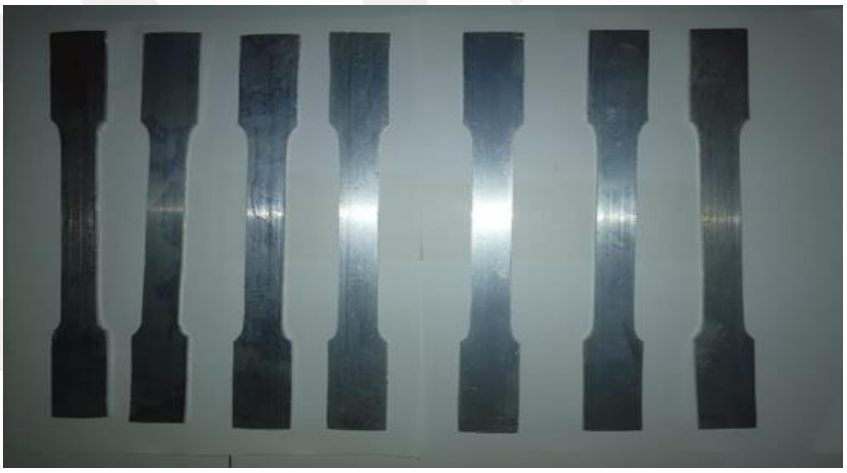

Figure 3.9 Aluminum coupon test specimens

Figure 3.10 ZWICK ROELL Z300E testing machine

Table 3.9 Dimensions of the aluminum coupon test specimens

Specimen	W2 (mm)	W1 (mm)	t (mm)	L1 (mm)	L2 (mm)
T1	18.98	29.7	2.14	120	57.42
T2	18.98	30.1	2.14	120	58.31
T3	18.98	30.5	2.14	120	59.93
T4	19.12	29.3	2.14	120	60.01
T5	19.11	29.1	2.14	120	59.21
T6	19.13	29.9	2.14	120	58.34
T7	19.22	30.7	2.14	120	57.58
T8	19.11	29.5	2.14	120	59.43
T9	18.95	29.4	2.14	120	59.78
T10	18.67	30.2	2.14	120	60.15

3.3.2 Compressive strength test

The compressive strength tests were performed to determine the ultimate compressive strengths of the composite specimens. The tests were carried out until a displacement of 15 mm for all the specimens is reached by applying a steady incremental force. The compressive strength test was carried out for the hollow circular aluminum tubes (HCAT), polymer concrete-filled aluminum tubes (PCFAT), and carbon fiber reinforced polymer concrete filled aluminum (CFPCFAT) tubes. Since the tested samples are composite assemblies, there are no standards. Therefore, the tests were carried out by considering previous studies such as [19] and [23]. The speed for the tests was 0.05 mm/min, and the testing machine is ALFA B-001 PC which matches the International Standards ASTM C39 [40] and EN 12390-4 [41], as shown in Fig. 3.11. All the loads were measured and recorded with a load cell that has a capacity of 100 tons. The test setup is shown in Fig.3.12. The compressive strength was calculated by the following equation.

$$\sigma = \frac{P}{A} \tag{3.1}$$

Here, σ refers to the compressive strength (MPa), P is the applied load (N), and A is the cross-sectional area of the specimen (mm^2).

Figure 3.11 ALFA B-001 PC testing machine

Figure 3.12 Test setup

3.3.3 Specimen preparation

3.3.3.1 Hollow circular aluminum tubes (HCAT)

Nine 6082-T6 aluminum tubes of 3m long each were purchased and moved to the laboratory. They were cut to the appropriate length by using (KAR METAL 300 ODG) cutting machine, as shown in Fig. 3.13. A total of 108 specimens were prepared. 36 of them were used in the tests performed for the determination of the compressive strength of HCATs.

Figure 3.13 Specimens cut using KAR METAL 300 ODG

In order to obtain the required thicknesses, OSTİM MAKİNA SN 50 type turning machine was used. The thickness of each sample was checked using a micrometer. The turning machine is shown in Fig. 3.14. In addition, the aluminum tubes prepared for the tests are shown in Fig. 3.15. Table 3.10 shows the sample diameters, lengths, and thicknesses and the ratios of length to diameter and thickness to diameter. In the first column of this table, HCAT refers to the hollow circular aluminum tubes, while the numbers 120, 150, 180, or 210 refer to the sample length, the next number (2, 3, or 4) defines the thickness, and the last number (1, 2, or 3) defines the sample number for that geometry.

Figure 3.14 OSTİM MAKİNA SN 50 turning machine

Figure 3.15 HCAT specimens

Table 3.10 Dimensions of HCAT specimens

Specimen	D (mm)	t (mm)	D/t	L (mm)	L/D	A_{al} (mm^2)	No.
HCAT120-2-1	40	2	20.0	120	3	238.64	3
HCAT120-2-2	40	2	20.0	120	3	238.64	3
HCAT120-2-3	40	2	20.0	120	3	238.64	3
HCAT120-3-1	40	3	13.3	120	3	348.54	3
HCAT120-3-2	40	3	13.3	120	3	348.54	3
HCAT120-3-3	40	3	13.3	120	3	348.54	3
HCAT120-4-1	40	4	10.0	120	3	452.16	3
HCAT120-4-2	40	4	10.0	120	3	452.16	3
HCAT120-4-3	40	4	10.0	120	3	452.16	3
HCAT150-2-1	50	2	25.0	150	3	301.44	3
HCAT150-2-2	50	2	25.0	150	3	301.44	3
HCAT150-2-3	50	2	25.0	150	3	301.44	3
HCAT150-3-1	50	3	16.7	150	3	442.74	3
HCAT150-3-2	50	3	16.7	150	3	442.74	3
HCAT150-3-3	50	3	16.7	150	3	442.74	3
HCAT150-4-1	50	4	12.5	150	3	577.76	3
HCAT150-4-2	50	4	12.5	150	3	577.76	3
HCAT150-4-3	50	4	12.5	150	3	577.76	3
HCAT180-2-1	60	2	30.0	180	3	364.24	3
HCAT180-2-2	60	2	30.0	180	3	364.24	3
HCAT180-2-3	60	2	30.0	180	3	364.24	3
HCAT180-3-1	60	3	20.0	180	3	536.94	3
HCAT180-3-2	60	3	20.0	180	3	536.94	3
HCAT180-3-3	60	3	20.0	180	3	536.94	3
HCAT180-4-1	60	4	15.0	180	3	703.36	3
HCAT180-4-2	60	4	15.0	180	3	703.36	3
HCAT180-4-3	60	4	15.0	180	3	703.36	3
HCAT210-2-1	70	2	35.0	210	3	427.04	3
HCAT210-2-2	70	2	35.0	210	3	427.04	3
HCAT210-2-3	70	2	35.0	210	3	427.04	3
HCAT210-3-1	70	3	23.3	210	3	631.14	3
HCAT210-3-2	70	3	23.3	210	3	631.14	3
HCAT210-3-3	70	3	23.3	210	3	631.14	3
HCAT210-4-1	70	4	17.5	210	3	828.96	3
HCAT210-4-2	70	4	17.5	210	3	828.96	3
HCAT210-4-3	70	4	17.5	210	3	828.96	3

In Table 3.10, D, t, and L refer to diameter, thickness, and length, respectively, while A_{al} represents the total cross-sectional area of the aluminum tube. It should be noted

that D/t ratio is taken as 3 for all specimens. As seen from this table, 3 specimens for each geometry are used for testing.

3.3.3.2 Polymer concrete-filled aluminum tubes (PCFAT)

72 of the hollow tubes were used to prepare PCFATs. PC mixture was prepared according to the predetermined proportions previously mentioned. Then, the PC was poured into the HCAT tubes. It should be noted that the HCAT tubes were covered from the bottom in order to prevent the PC parting from the HCAT tubes. The prepared PCFAT specimens are shown in Fig. 3.16, and the dimensions of the specimens are given in Table 3.11. In this table, A_{pc} represents the cross-sectional area of polymer concrete.

Figure 3.16 PCFAT specimen

Table 3.11 Dimensions of PCFAT specimens

Specimen	D (mm)	t (mm)	D/t	L (mm)	L/D	A_{pc} (mm^2)	A_{al} (mm^2)	No.
PCFAT120-2-1	40	2	20.00	120	3	1017.36	238.64	3
PCFAT120-2-2	40	2	20.00	120	3	1017.36	238.64	3
PCFAT120-2-3	40	2	20.00	120	3	1017.36	238.64	3
PCFAT120-3-1	40	3	13.33	120	3	907.46	348.54	3
PCFAT120-3-2	40	3	13.33	120	3	907.46	348.54	3
PCFAT120-3-3	40	3	13.33	120	3	907.46	348.54	3
PCFAT120-4-1	40	4	10.00	120	3	803.84	452.16	3
PCFAT120-4-2	40	4	10.00	120	3	803.84	452.16	3
PCFAT120-4-3	40	4	10.00	120	3	803.84	452.16	3
PCFAT150-2-1	50	2	25.00	150	3	1661.06	301.44	3
PCFAT150-2-2	50	2	25.00	150	3	1661.06	301.44	3
PCFAT150-2-3	50	2	25.00	150	3	1661.06	301.44	3
PCFAT150-3-1	50	3	16.67	150	3	1519.76	442.74	3
PCFAT150-3-2	50	3	16.67	150	3	1519.76	442.74	3
PCFAT150-3-3	50	3	16.67	150	3	1519.76	442.74	3
PCFAT150-4-1	50	4	12.50	150	3	1384.74	577.76	3
PCFAT150-4-2	50	4	12.50	150	3	1384.74	577.76	3
PCFAT150-4-3	50	4	12.50	150	3	1384.74	577.76	3
PCFAT180-2-1	60	2	30.00	180	3	2461.76	364.24	3
PCFAT180-2-2	60	2	30.00	180	3	2461.76	364.24	3
PCFAT180-2-3	60	2	30.00	180	3	2461.76	364.24	3
PCFAT180-3-1	60	3	20.00	180	3	2289.06	536.94	3
PCFAT180-3-2	60	3	20.00	180	3	2289.06	536.94	3
PCFAT180-3-3	60	3	20.00	180	3	2289.06	536.94	3
PCFAT180-4-1	60	4	15.00	180	3	2122.64	703.36	3
PCFAT180-4-2	60	4	15.00	180	3	2122.64	703.36	3
PCFAT180-4-3	60	4	15.00	180	3	2122.64	703.36	3
PCFAT210-2-1	70	2	35.00	210	3	3419.46	427.04	3
PCFAT210-2-2	70	2	35.00	210	3	3419.46	427.04	3
PCFAT210-2-3	70	2	35.00	210	3	3419.46	427.04	3
PCFAT210-3-1	70	3	23.33	210	3	3215.36	631.14	3
PCFAT210-3-2	70	3	23.33	210	3	3215.36	631.14	3
PCFAT210-3-3	70	3	23.33	210	3	3215.36	631.14	3
PCFAT210-4-1	70	4	17.50	210	3	3017.54	828.96	3
PCFAT210-4-2	70	4	17.50	210	3	3017.54	828.96	3
PCFAT210-4-3	70	4	17.50	210	3	3017.54	828.96	3

3.3.3.3 Carbon fiber reinforced polymer concrete filled aluminum tubes (CFPCFAT)

After waiting for the time required for the curing of the PCFAT samples, 36 samples of them were used to produce carbon fiber reinforced polymer concrete filled aluminum tubes (CFPCFAT). The process of applying carbon fiber was carried out according to the instructions recommended by Sika Company. Because of the cold weather that reached below zero centigrade in the working period, the production was started with putting all tools and materials used into the oven with a temperature of 25 °C to match the room temperature. After removal from the oven, the epoxy was mixed, and by using a brush, two layers of epoxy, first on the outside surface of PCFAT tubes and the second on the carbon fiber, was wrapped tightly. To avoid any contact between the samples and any other surface, the sample was fixed on both sides using a carpentry clamp, as shown in Fig. 3.17. Then, a layer of epoxy was placed on the outer surface of the carbon fiber. The final form of the specimens can be seen in Fig. 3.18. The sample dimensions are listed in Table 3.12. In this table, A_{cf} represents the cross-sectional area of the carbon fiber layer.

Figure 3.17 Preperation of (CFPCFAT) specimens

Figure 3.18 CFPCFAT specimens

Table 3.12 Dimensions of CFPCFAT specimens

Specimen	D (mm)	t (mm)	D/t	L (mm)	L/D	A_{cf} (mm^2)	A_{pc} (mm^2)	A_{al} (mm^2)	No.
CFPCFAT120-2-1	40	2	20.00	120	3	16.20	1017.36	238.64	3
CFPCFAT120-2-2	40	2	20.00	120	3	16.20	1017.36	238.64	3
CFPCFAT120-2-3	40	2	20.00	120	3	16.20	1017.36	238.64	3
CFPCFAT120-3-1	40	3	13.33	120	3	16.20	907.46	348.54	3
CFPCFAT120-3-2	40	3	13.33	120	3	16.20	907.46	348.54	3
CFPCFAT120-3-3	40	3	13.33	120	3	16.20	907.46	348.54	3
CFPCFAT120-4-1	40	4	10.00	120	3	16.20	803.84	452.16	3
CFPCFAT120-4-2	40	4	10.00	120	3	16.20	803.84	452.16	3
CFPCFAT120-4-3	40	4	10.00	120	3	16.20	803.84	452.16	3
CFPCFAT150-2-1	50	2	25.00	150	3	20.25	1661.06	301.44	3
CFPCFAT150-2-2	50	2	25.00	150	3	20.25	1661.06	301.44	3
CFPCFAT150-2-3	50	2	25.00	150	3	20.25	1661.06	301.44	3
CFPCFAT150-3-1	50	3	16.67	150	3	20.25	1519.76	442.74	3
CFPCFAT150-3-2	50	3	16.67	150	3	20.25	1519.76	442.74	3
CFPCFAT150-3-3	50	3	16.67	150	3	20.25	1519.76	442.74	3
CFPCFAT150-4-1	50	4	12.50	150	3	20.25	1384.74	577.76	3
CFPCFAT150-4-2	50	4	12.50	150	3	20.25	1384.74	577.76	3
CFPCFAT150-4-3	50	4	12.50	150	3	20.25	1384.74	577.76	3
CFPCFAT180-2-1	60	2	30.00	180	3	24.30	2461.76	364.24	3
CFPCFAT180-2-2	60	2	30.00	180	3	24.30	2461.76	364.24	3
CFPCFAT180-2-3	60	2	30.00	180	3	24.30	2461.76	364.24	3
CFPCFAT180-3-1	60	3	20.00	180	3	24.30	2289.06	536.94	3
CFPCFAT180-3-2	60	3	20.00	180	3	24.30	2289.06	536.94	3
CFPCFAT180-3-3	60	3	20.00	180	3	24.30	2289.06	536.94	3
CFPCFAT180-4-1	60	4	15.00	180	3	24.30	2122.64	703.36	3
CFPCFAT180-4-2	60	4	15.00	180	3	24.30	2122.64	703.36	3
CFPCFAT180-4-3	60	4	15.00	180	3	24.30	2122.64	703.36	3
CFPCFAT210-2-1	70	2	35.00	210	3	28.35	3419.46	427.04	3
CFPCFAT210-2-2	70	2	35.00	210	3	28.35	3419.46	427.04	3
CFPCFAT210-2-3	70	2	35.00	210	3	28.35	3419.46	427.04	3
CFPCFAT210-3-1	70	3	23.33	210	3	28.35	3215.36	631.14	3
CFPCFAT210-3-2	70	3	23.33	210	3	28.35	3215.36	631.14	3
CFPCFAT210-3-3	70	3	23.33	210	3	28.35	3215.36	631.14	3
CFPCFAT210-4-1	70	4	17.50	210	3	28.35	3017.54	828.96	3
CFPCFAT210-4-2	70	4	17.50	210	3	28.35	3017.54	828.96	3
CFPCFAT210-4-3	70	4	17.50	210	3	28.35	3017.54	828.96	3

CHAPTER 4

RESULTS AND DISCUSSIONS

4.1 Introduction

In this chapter we discuss the results of the experiments mentioned in the previous chapter. The results of the aluminum coupon tests are presented first. Then, we determined the compressive strength and the axial stiffness values with the corresponding failure modes. In addition, two different models based on the ultimate load capacities are used to make comparisons between the experimental and numerical results.

4.2 Aluminum coupon test results

In this section, the aluminum coupon test results are summarized. Table 4.1 summarizes the coupon test results, and the true stress-strain curves for the aluminum coupon test specimens are given in Fig. 4.1. Each tested specimens have similar loading conditions and displacement speed. Standard sized samples were prepared from a 6082-T6 aluminum plates which have the same composition with the aluminum tubes. The deformation rate is 10mm/min until the reduction in force and 500mm/min for travel after the break. Using the dimensions of each sample and the machine's data, % uniform elongation values, elastic moduli, and strain hardening exponents are obtained.

It should be noted that there is a slight variation between the specimen dimensions due to the manual preparation method, which may lead to disparity in the collected results.

Table 4.1 Coupon test results

Specimen	S_0 (mm^2)	E (GPa)	$Rp_{0.2}$ (MPa)	Rm (MPa)	Ag (%)	n
T1	40.62	85	267.19	290.74	4.84	0.067
T2	40.62	67.1	265.76	282.91	2.83	-
T3	40.62	69.1	260.03	288.43	6.40	0.071
T4	40.92	66.1	285.12	301.94	4.34	0.052
T5	40.90	66.4	269.96	293.14	4.95	0.062
T6	40.94	77.0	225.96	259.35	3.70	0.081
T7	41.13	69.0	227.13	262.20	5.32	0.085
T8	40.90	68.8	214.97	250.91	4.82	0.092
T9	40.55	81.3	213.68	254.06	5.27	0.096
T10	39.95	73.5	214.53	255.69	6.20	0.095

In Table 4.1,, S_0 refers to the initial cross-sectional area. E refers to the elasticity modulus, Rm, $Rp_{0.2}$ refers to the tensile strength and proof stress at non-proportional elongation at 0.2% strain, respectively, Ag represents the uniform elongation, and n refers to the strain hardening exponent.

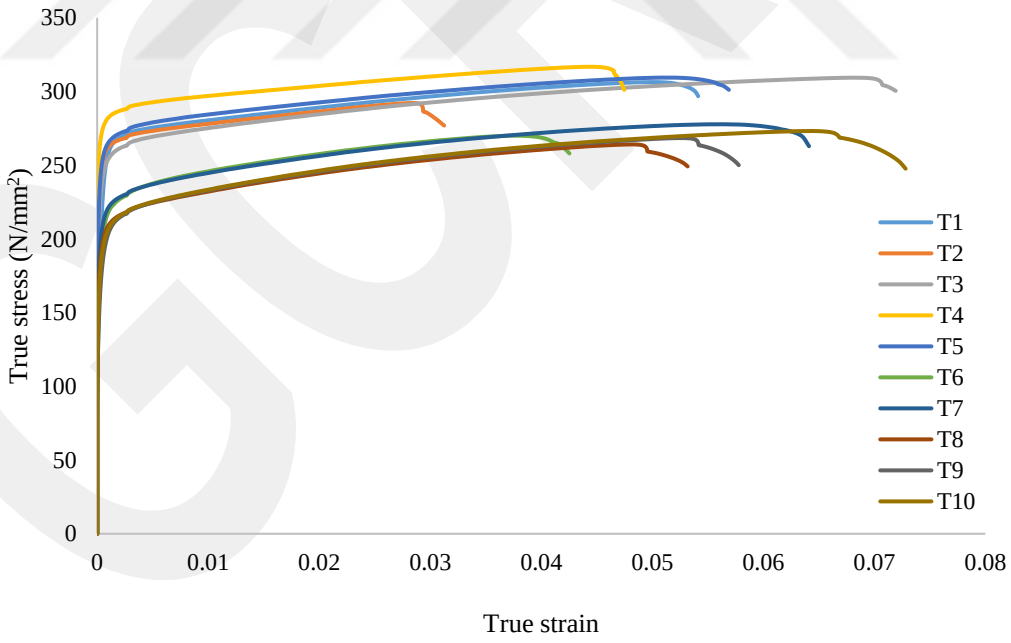

Figure 4.1 True stress-strain curves for the aluminum coupon test

4.3 Compressive strength test results

The behaviour of PCFATs are influenced by the difference between the Poisson's ratio of polymer concrete and the aluminum tube. Since the Poisson's ratio of concrete is slightly lower than that of aluminum, the tube is separated from the polymer concrete core in the initial loading stages. However, with the increasing axial load, the lateral deformation of concrete catches the deformation of the aluminum tube, which develops tensile hoop stress. The confining effect imposed by the aluminum tube on polymer concrete results in a notable increase in the specimen axial load capacity. The load-carrying capacity of HCAT tubes under axial compression is affected by the diameter and thickness. The load-carrying capacity increases with increasing thickness, and decreases with decreasing diameter. The carbon fiber reinforcement around the aluminum tubes does not affect all mechanical properties of the specimens, however it increases the load-carrying capacity of PCFATs and diminishes the thickness effect of aluminum tubes.

4.3.1 Compression test results of HCAT specimens

The results of compression tests for HCAT specimens as well as the load-displacement graphs are presented in this part. Table 4.2 shows the ultimate load capacity of the specimens, while Fig. 4.2 gives the mean ultimate load capacity of the specimens.

Table 4.2 Axial load capacity of HCAT specimens

Specimen	D (mm)	t (mm)	L (mm)	Ultimate load capacity (kN)	Mean (kN)	Standard deviation (kN)
HCAT120-2-1	40	2	120	68.605		
HCAT120-2-2	40	2	120	69.529	70.397	2.35
HCAT120-2-3	40	2	120	73.057		
HCAT120-3-1	40	3	120	107.250		
HCAT120-3-2	40	3	120	102.445	103.677	3.14
HCAT120-3-3	40	3	120	101.336		
HCAT120-4-1	40	4	120	142.872		
HCAT120-4-2	40	4	120	143.107	142.867	0.24
HCAT120-4-3	40	4	120	142.620		
HCAT150-2-1	50	2	150	118.744		
HCAT150-2-2	50	2	150	117.601	117.198	1.78
HCAT150-2-3	50	2	150	115.249		
HCAT150-3-1	50	3	150	184.828		
HCAT150-3-2	50	3	150	176.057	178.684	5.34
HCAT150-3-3	50	3	150	175.166		
HCAT150-4-1	50	4	150	235.538		
HCAT150-4-2	50	4	150	235.319	235.891	0.81
HCAT150-4-3	50	4	150	236.815		
HCAT180-2-1	60	2	180	104.781		
HCAT180-2-2	60	2	180	66.656	77.841	23.44
HCAT180-2-3	60	2	180	62.085		
HCAT180-3-1	60	3	180	160.801		
HCAT180-3-2	60	3	180	161.204	161.803	1.40
HCAT180-3-3	60	3	180	163.405		
HCAT180-4-1	60	4	180	223.189		
HCAT180-4-2	60	4	180	223.003	221.474	2.81
HCAT180-4-3	60	4	180	218.231		
HCAT210-2-1	70	2	210	136.907		
HCAT210-2-2	70	2	210	142.267	141.578	4.37
HCAT210-2-3	70	2	210	145.560		
HCAT210-3-1	70	3	210	214.955		
HCAT210-3-2	70	3	210	215.492	214.613	1.09
HCAT210-3-3	70	3	210	213.393		
HCAT210-4-1	70	4	210	287.054		
HCAT210-4-2	70	4	210	286.081	285.783	1.44
HCAT210-4-3	70	4	210	284.215		

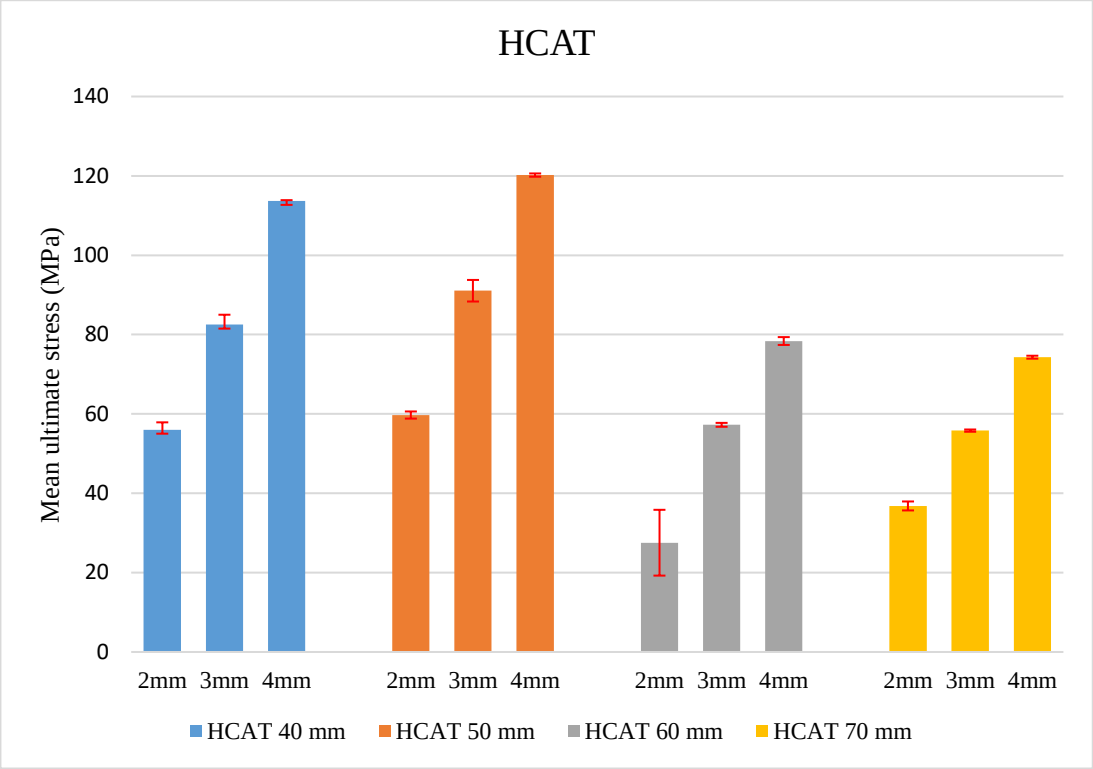

Figure 4.2 Mean ultimate lad capacity of HCAT Specimens

The load carrying capacity depends on mainly thickness, length, and diameter of the tubes. A general increase in the load-carrying capacity is noted with the increase in the thickness of all the specimens. For example, on average there is an 107.86 % increase in the load carrying capacity for specimen HCAT180 (D = 60 mm) is noted when its thickness increases from 2 mm to 3 mm, and the average increase is 36.88 % when the thickness is 4 mm. In addition, an increase of 66.48 % is observed when the diameter increases from 40 mm to 50 mm for the 2 mm thickness. Once the thickness is increased to 4 mm, the load carrying capacity is increased further 65.11 %. The thickness effect can be readily detected in the load-displacement diagrams. Fig 4.3 and 4.4 shows load-displacement diagrams of some samples of HCAT120 (D = 40 mm) and HCAT180 (D = 60 mm) with 2, 3, and 4 mm thickness values respectively. However, there is a noticeable decrease of 35.58 % in the mean ultimate load capacities when the diameter changes from 50 mm to 60 mm for a constant thickness of 2 mm.

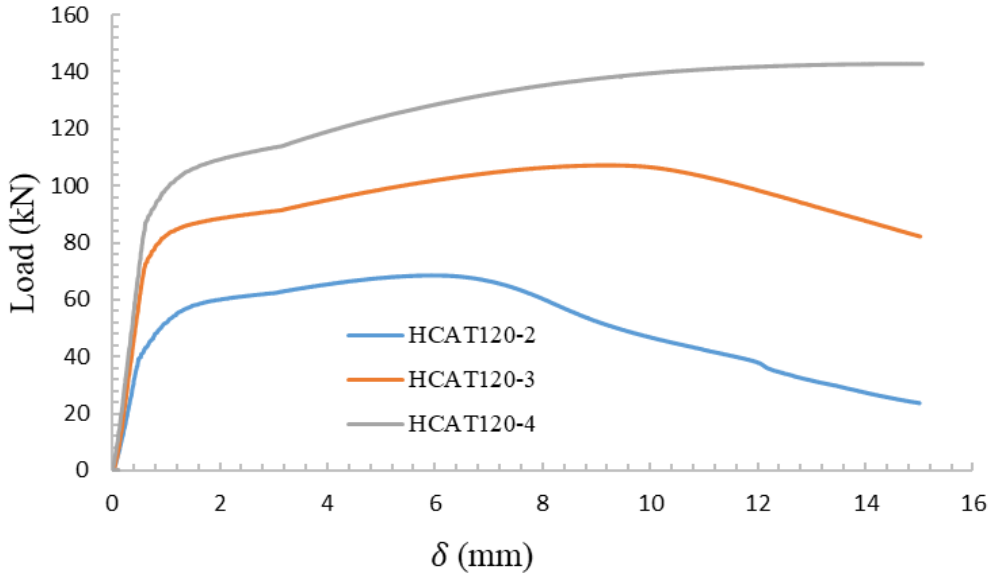

Figure 4.3 Load-displacement curves for HCAT120 specimens (D = 40 mm)

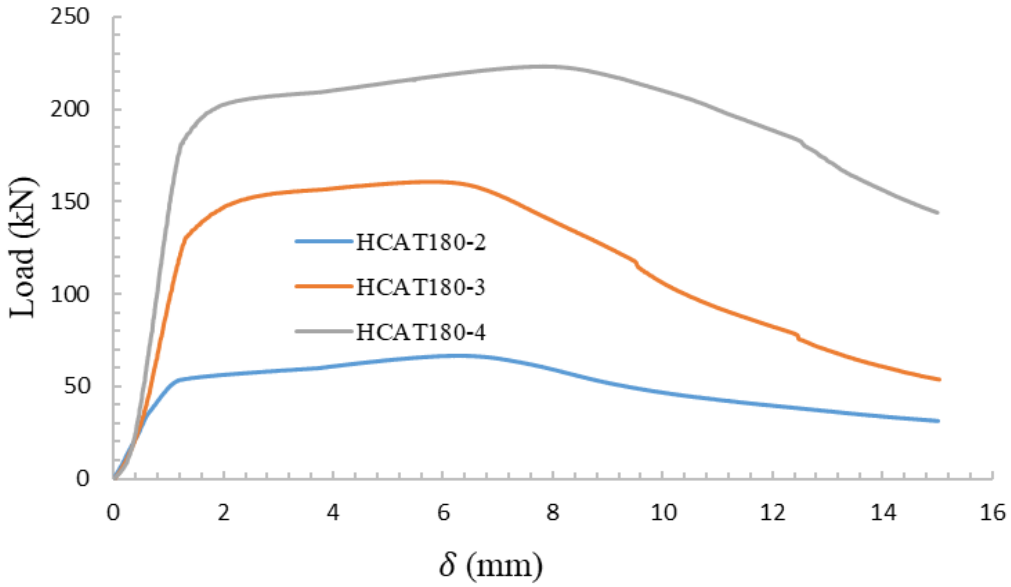

Figure 4.4 Load-displacement curves for HCAT180 specimens (D = 60 mm)

4.3.2 Compression test results of PCFAT specimens

36 PCFAT specimens were tested under compression. Each specimen was tested with similar loading conditions and displacement speed. The ultimate stress for each specimen was averaged for further analysis. Table 4.3 shows the PCFAT compression test results, and Fig. 4.5 shows the mean ultimate stress values.

Table 4.3 Axial load capacity of PCFAT specimens

Specimen	D (mm)	t (mm)	L (mm)	Ultimate load capacity (kN)	Ultimate stress (MPa)	Mean (MPa)	Standard deviation (MPa)
PCFAT120-2-1	40	2	120	126.25	100.47		
PCFAT120-2-2	40	2	120	127.28	101.29	101.31	0.84
PCFAT120-2-3	40	2	120	128.39	102.17		
PCFAT120-3-1	40	3	120	164.63	131.01		
PCFAT120-3-2	40	3	120	164.31	130.76	132.19	2.26
PCFAT120-3-3	40	3	120	169.40	134.81		
PCFAT120-4-1	40	4	120	191.35	152.27		
PCFAT120-4-2	40	4	120	185.50	147.62	150.58	2.57
PCFAT120-4-3	40	4	120	190.81	151.84		
PCFAT150-2-1	50	2	150	245.32	125.00		
PCFAT150-2-2	50	2	150	242.48	123.56	120.13	7.23
PCFAT150-2-3	50	2	150	219.44	111.82		
PCFAT150-3-1	50	3	150	289.52	147.53		
PCFAT150-3-2	50	3	150	274.85	140.11	142.59	4.28
PCFAT150-3-3	50	3	150	274.97	140.11		
PCFAT150-4-1	50	4	150	339.41	172.95		
PCFAT150-4-2	50	4	150	343.86	175.22	173.41	1.63
PCFAT150-4-3	50	4	150	337.65	172.05		
PCFAT180-2-1	60	2	180	284.20	100.57		
PCFAT180-2-2	60	2	180	230.75	81.65	92.15	9.62
PCFAT180-2-3	60	2	180	266.34	94.25		
PCFAT180-3-1	60	3	180	328.51	116.24		
PCFAT180-3-2	60	3	180	320.48	113.40	113.28	3.03
PCFAT180-3-3	60	3	180	311.38	110.19		
PCFAT180-4-1	60	4	180	364.80	129.09		
PCFAT180-4-2	60	4	180	366.21	129.59	129.13	0.43
PCFAT180-4-3	60	4	180	363.77	128.72		
PCFAT210-2-1	70	2	210	308.16	80.11		
PCFAT210-2-2	70	2	210	309.00	80.33	80.26	0.13
PCFAT210-2-3	70	2	210	309.05	80.35		
PCFAT210-3-1	70	3	210	364.80	94.84		
PCFAT210-3-2	70	3	210	362.48	94.24	95.28	1.32
PCFAT210-3-3	70	3	210	372.23	96.77		
PCFAT210-4-1	70	4	210	485.48	126.21		
PCFAT210-4-2	70	4	210	478.55	124.41	126.39	2.06
PCFAT210-4-3	70	4	210	494.43	128.54		

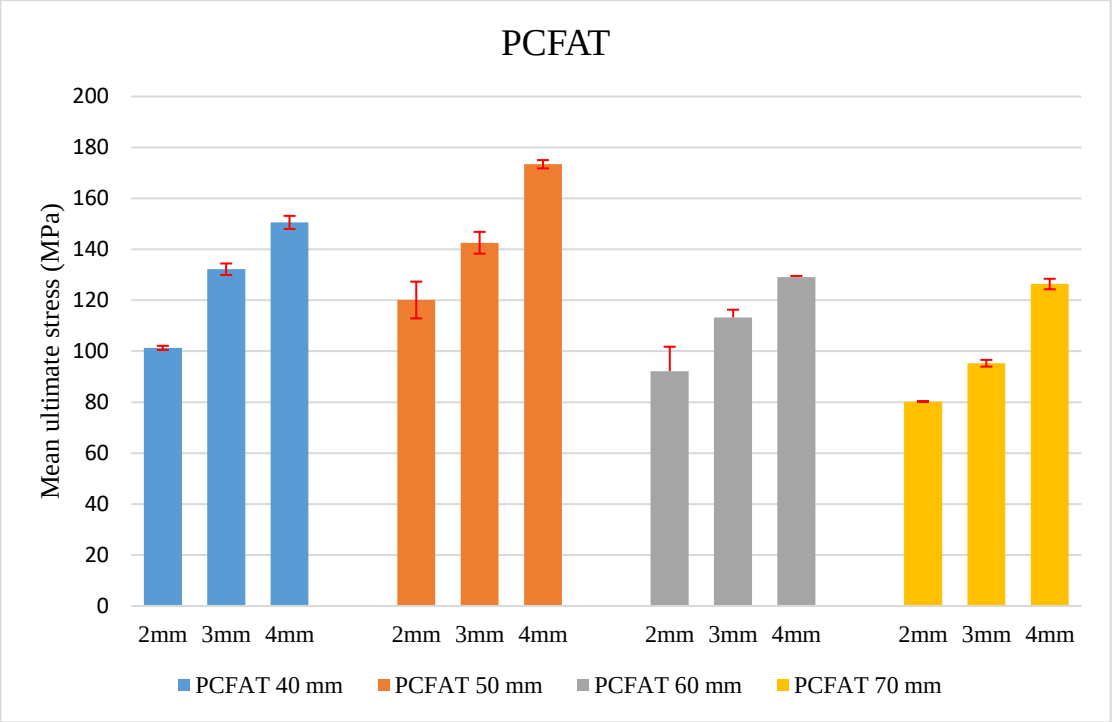

Figure 4.5 Mean ultimate stresses of PCFAT specimens

When high strength polymer concrete and thin-walled aluminum tubes are used together, the relatively brittle nature of polymer concrete is partially mitigated by the confinement of the aluminum tube. Besides, local buckling of the thin aluminum tube is delayed by the support of the polymer concrete. An increase in the load-carrying capacity is noted with the increasing thicknesses of all the specimens as shown in Table. 4.3. For instance, an average increase of 18.38 % in the load carrying capacity is detected when the thickness is increased from 2 mm to 3 mm for PCFAT180 specimens (D = 60 mm). In addition, when the diameter increases from 40 mm to 50 mm, a general increase of 77.38 % in the load-carrying capacity is observed for the 4 mm thickness specimens. However, when the diameter is increased from 50 mm to 60 mm, there is a decrease by 19.06 % in mean ultimate stress for 3mm thickness specimens.

4.3.3 Compression test results of CFPCFAT specimens

In this section, the results of 36 CFPCFAT specimens tested under compression are summarized. Each specimen was tested with similar loading conditions and displacement speed. The stress values corresponding to each dimension are tabulated

in Table 4.4, and Fig 4.6 demonstrates the mean ultimate stresses of CFPCFAT specimens as bar charts.

Table 4.4 Axial load capacity of CFPCFAT specimens

Specimen	D (mm)	t (mm)	L (mm)	Ultimate load capacity (kN)	Ultimate stress (MPa)	Mean (MPa)	Standard deviation (MPa)
CFPCFAT120-2-1	40	2	120	180.812	143.886		
CFPCFAT120-2-2	40	2	120	181.669	144.568	145.865	2.85
CFPCFAT120-2-3	40	2	120	187.415	149.141		
CFPCFAT120-3-1	40	3	120	215.470	166.991		
CFPCFAT120-3-2	40	3	120	216.215	171.470	170.173	2.77
CFPCFAT120-3-3	40	3	120	209.846	172.058		
CFPCFAT120-4-1	40	4	120	229.321	182.488		
CFPCFAT120-4-2	40	4	120	222.214	176.832	181.285	3.98
CFPCFAT120-4-3	40	4	120	231.890	184.534		
CFPCFAT150-2-1	50	2	150	265.010	135.037		
CFPCFAT150-2-2	50	2	150	263.095	134.061	135.807	2.23
CFPCFAT150-2-3	50	2	150	271.462	138.324		
CFPCFAT150-3-1	50	3	150	296.498	151.082		
CFPCFAT150-3-2	50	3	150	297.372	151.527	153.887	4.47
CFPCFAT150-3-3	50	3	150	312.141	159.053		
CFPCFAT150-4-1	50	4	150	345.197	175.897		
CFPCFAT150-4-2	50	4	150	358.993	182.926	178.956	3.6
CFPCFAT150-4-3	50	4	150	349.414	178.045		
CFPCFAT180-2-1	60	2	180	303.337	107.338		
CFPCFAT180-2-2	60	2	180	304.182	107.637	108.562	1.86
CFPCFAT180-2-3	60	2	180	312.866	110.710		
CFPCFAT180-3-1	60	3	180	342.796	121.301		
CFPCFAT180-3-2	60	3	180	310.922	110.022	116.601	5.86
CFPCFAT180-3-3	60	3	180	334.827	118.481		
CFPCFAT180-4-1	60	4	180	364.594	129.014		
CFPCFAT180-4-2	60	4	180	333.315	117.946	126.436	7.53
CFPCFAT180-4-3	60	4	180	374.018	132.349		
CFPCFAT210-2-1	70	2	210	451.300	117.327		
CFPCFAT210-2-2	70	2	210	439.706	114.313	114.254	3.1
CFPCFAT210-2-3	70	2	210	427.423	111.120		
CFPCFAT210-3-1	70	3	210	470.001	122.189		
CFPCFAT210-3-2	70	3	210	497.857	129.431	126.138	3.66
CFPCFAT210-3-3	70	3	210	487.712	126.794		
CFPCFAT210-4-1	70	4	210	521.836	135.665		
CFPCFAT210-4-2	70	4	210	511.480	132.973	133.947	1.49
CFPCFAT210-4-3	70	4	210	512.367	133.204		

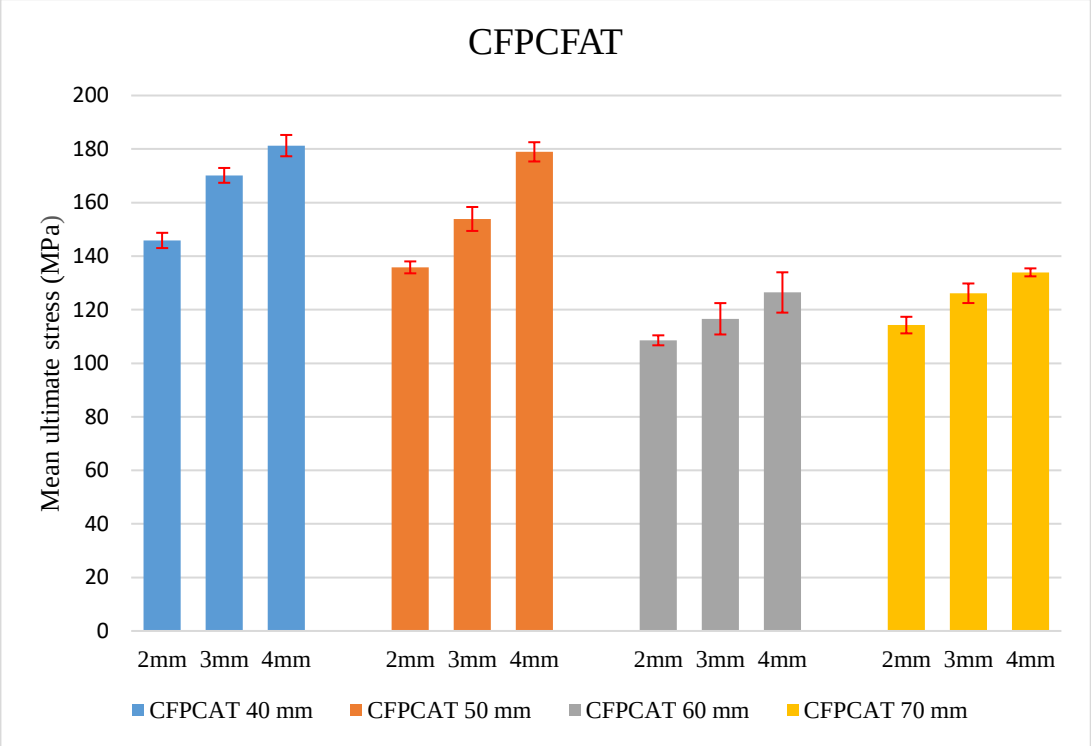

Figure 4.6 Mean ultimate stresses of CFPCFAT specimens

The results show that there is an increase in the compressive strength of all specimens when carbon fiber reinforcement is used. For example, for specimens with 50 mm in diameter and 2, 3, and 4 mm in thickness, a significant increase in compressive strength compared to PCFATs with the same dimensions is noted. The effect of using carbon fiber wraps around aluminum tubes decreases with increasing length and diameter, though there is a very slight increase for the specimens with D = 70 mm. Compared to the previous results obtained from compression tests of HCATs and PCFATs, it is evident that there is an improvement in compressive strength for all the specimens. It is worth noting that the highest increase is observed for samples with 2mm thickness, which reduces the gap in the compressive strength for the specimens of similar dimensions. This is particularly important when lighter and thinner aluminum tubular structures are desired to be used as confinement because of cost and weight purposes. Table 4.5 shows the % load capacity increase of CFPCFAT compared to PCFAT specimens.

Table 4.5 Capacity increase of CFPCAT specimens

Specimen	Mean ultimate load capacity (kN)	Specimen	Mean ultimate load capacity (kN)	Capacity increase (%)
PCFAT120-2-1		CFPCFAT120-2-1		
PCFAT120-2-2	127.31	CFPCFAT120-2-2	183.30	43.98
PCFAT120-2-3		CFPCFAT120-2-3		
PCFAT120-3-1		CFPCFAT120-3-1		
PCFAT120-3-2	166.12	CFPCFAT120-3-2	213.84	28.73
PCFAT120-3-3		CFPCFAT120-3-3		
PCFAT120-4-1		CFPCFAT120-4-1		
PCFAT120-4-2	189.22	CFPCFAT120-4-2	227.81	20.39
PCFAT120-4-3		CFPCFAT120-4-3		
PCFAT150-2-1		CFPCFAT150-2-1		
PCFAT150-2-2	235.75	CFPCFAT150-2-2	266.52	13.06
PCFAT150-2-3		CFPCFAT150-2-3		
PCFAT150-3-1		CFPCFAT150-3-1		
PCFAT150-3-2	279.78	CFPCFAT150-3-2	302.00	7.94
PCFAT150-3-3		CFPCFAT150-3-3		
PCFAT150-4-1		CFPCFAT150-4-1		
PCFAT150-4-2	340.31	CFPCFAT150-4-2	351.20	3.20
PCFAT150-4-3		CFPCFAT150-4-3		
PCFAT180-2-1		CFPCFAT180-2-1		
PCFAT180-2-2	260.43	CFPCFAT180-2-2	306.79	17.80
PCFAT180-2-3		CFPCFAT180-2-3		
PCFAT180-3-1		CFPCFAT180-3-1		
PCFAT180-3-2	320.12	CFPCFAT180-3-2	329.52	2.93
PCFAT180-3-3		CFPCFAT180-3-3		
PCFAT180-4-1		CFPCFAT180-4-1		
PCFAT180-4-2	364.93	CFPCFAT180-4-2	367.54	0.71
PCFAT180-4-3		CFPCFAT180-4-3		
PCFAT210-2-1		CFPCFAT210-2-1		
PCFAT210-2-2	308.74	CFPCFAT210-2-2	439.48	42.35
PCFAT210-2-3		CFPCFAT210-2-3		
PCFAT210-3-1		CFPCFAT210-3-1		
PCFAT210-3-2	366.50	CFPCFAT210-3-2	485.19	32.38
PCFAT210-3-3		CFPCFAT210-3-3		
PCFAT210-4-1		CFPCFAT210-4-1		
PCFAT210-4-2	486.15	CFPCFAT210-4-2	515.23	5.98
PCFAT210-4-3		CFPCFAT210-4-3		

4.3.4 Stress-strain diagrams

The engineering stress-strain diagrams of PCFAT and CFPCFAT specimens under axial compressive loads are presented in this section. It should be noted that the comparison is made between the specimens that have the same tubular dimensions.

4.3.4.1 Compression test results for specimens with 40 mm diameter

The engineering stress-strain curves of the specimens confined with 40 mm diameter aluminum tubes having 2, 3 and 4 mm thickness and 120 mm length with and without carbon fiber wrap are presented in this section. As stated before, diameter to length ratio is kept constant at 1/3.

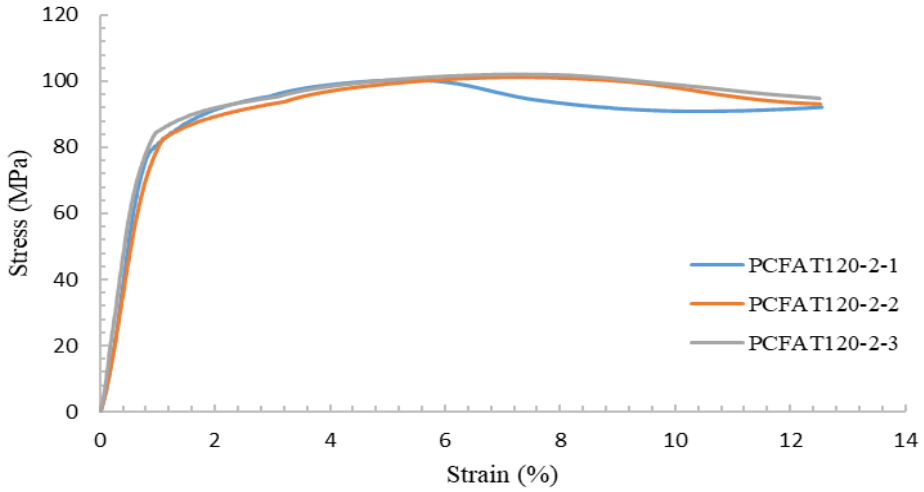

(a)

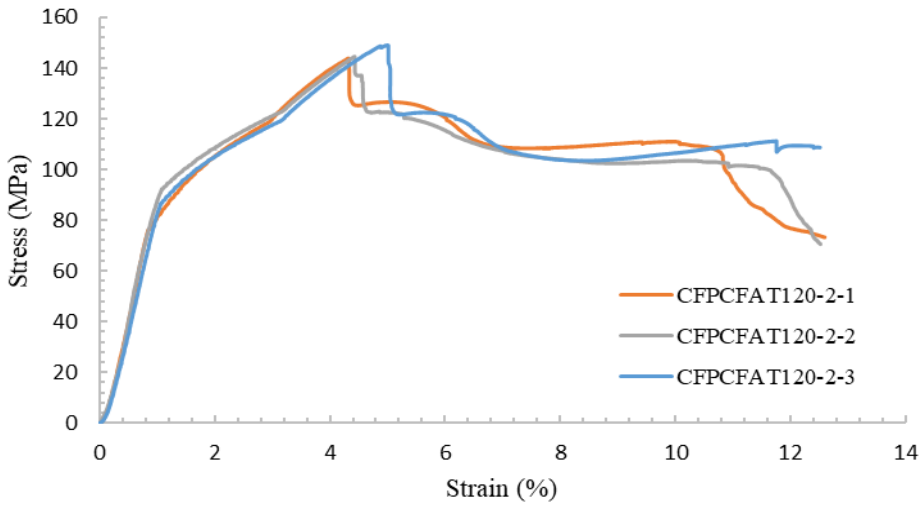

(b)

Figure 4.7 Stress-strain curves of (a) polymer concrete filled aluminum tube (PCFAT) and (b) carbon fiber wrapped PCFAT specimens having 40 mm diameter and 2 mm thickness

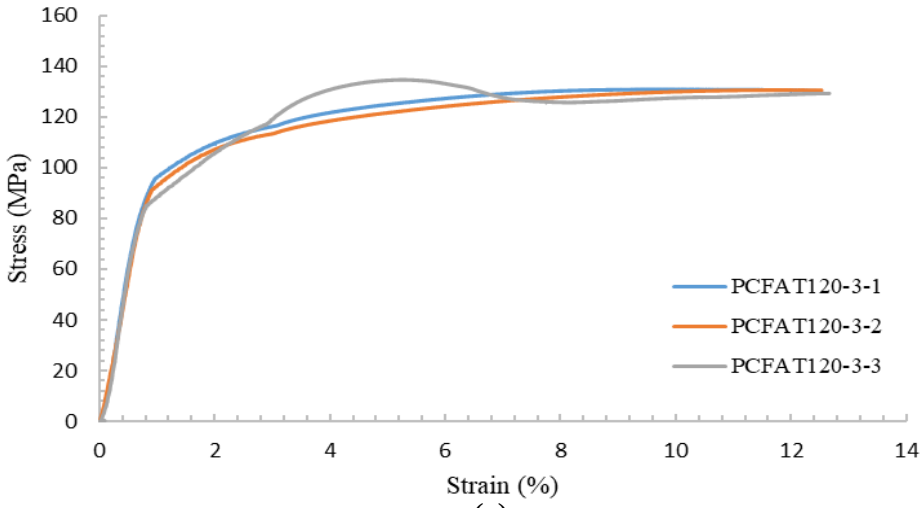

(a)

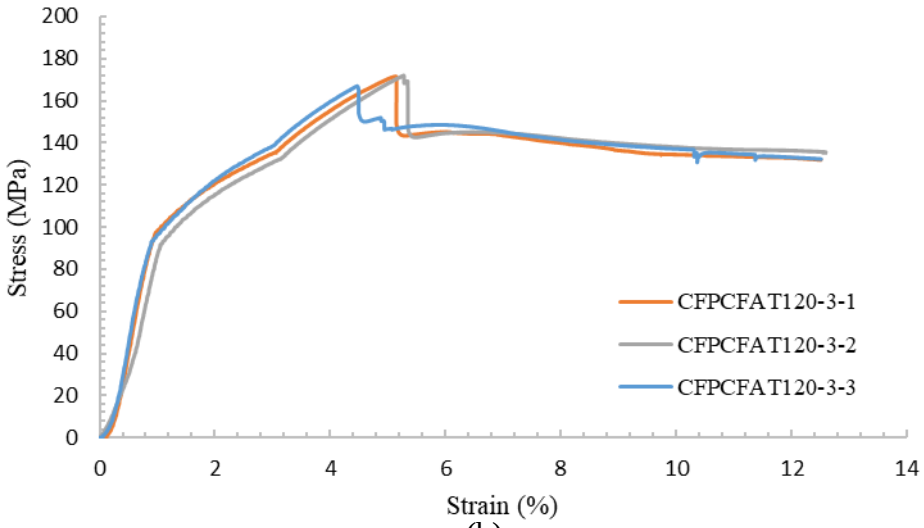

(b)

Figure 4.8 Stress-strain curves of (a) polymer concrete filled aluminum tube (PCFAT) and (b) carbon fiber wrapped PCFAT specimens having 40 mm diameter and 3 mm thickness

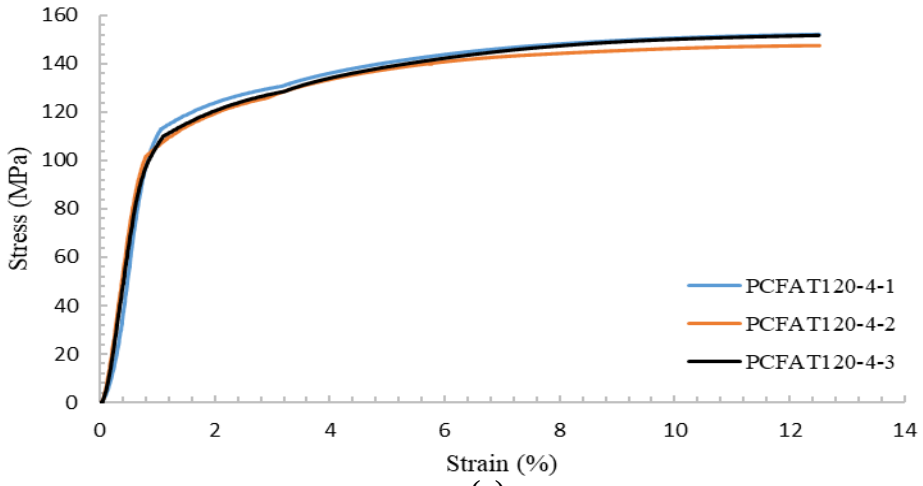

(a)

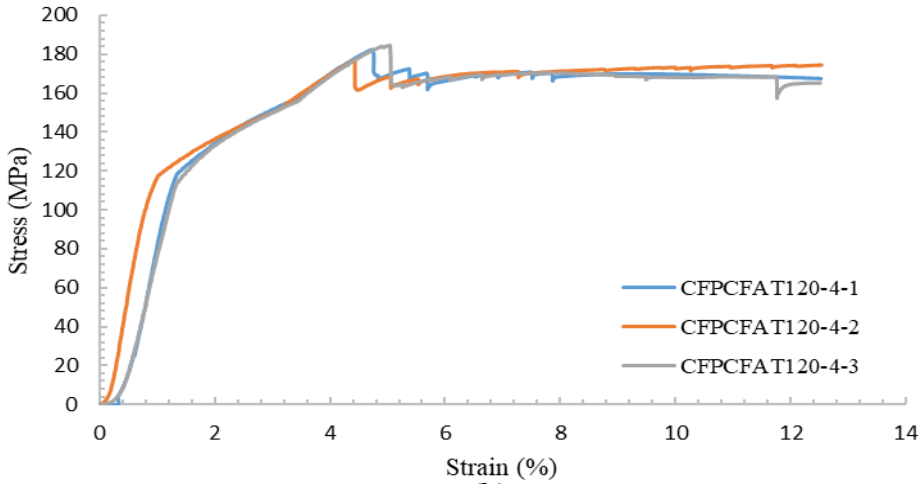

(b)

Figure 4.9 Stress-strain curves of (a) polymer concrete filled aluminum tube (PCFAT) and (b) carbon fiber wrapped PCFAT specimens having 40 mm diameter and 4 mm thickness

Fig. 4.7 shows typical stress-strain curves for PCFATs and CFPCFATs with 40 mm diameter and 2 mm thickness. The engineering stress is expressed as the applied load divided by the total original cross-sectional area of the specimen. Evidently, the strength and stiffness of polymer concrete cylinder is considerably increased when combined with aluminum tube because of the confinement effect. The axial stress increases at earlier stages of loading since the load is applied in longitudinal direction. The stress-strain curves of PCFATs are different from CFPCFATs specimens. This is reasonable since CFPCFATs have extra confinement with carbon fiber. The curve of PCFATs is ascending gradually to the peak point after some loading period, then the stress starts decreasing slowly. On the contrary, for CFPCFATs, the peak point appears

in an early stage of loading, then a sudden drop in stress occurs due to the carbon fiber rupture, and later stress decreases gradually, as shown in Figs. 4.8 and 4.9. The effect of thickness is more evident with thicker specimens since following peak stress, the drop in the stress after the peak point becomes less intense for both PCFAT and CFPCFAT specimens.

4.3.4.2 Compression test results for specimens with 50 mm diameter

The engineering stress-strain curves of the specimens confined with 50 mm diameter aluminum tubes having 2, 3 and 4 mm thickness and 150 mm length with and without carbon fiber wrap is presented in this section. Diameter to length ratio is kept constant at 1/3.

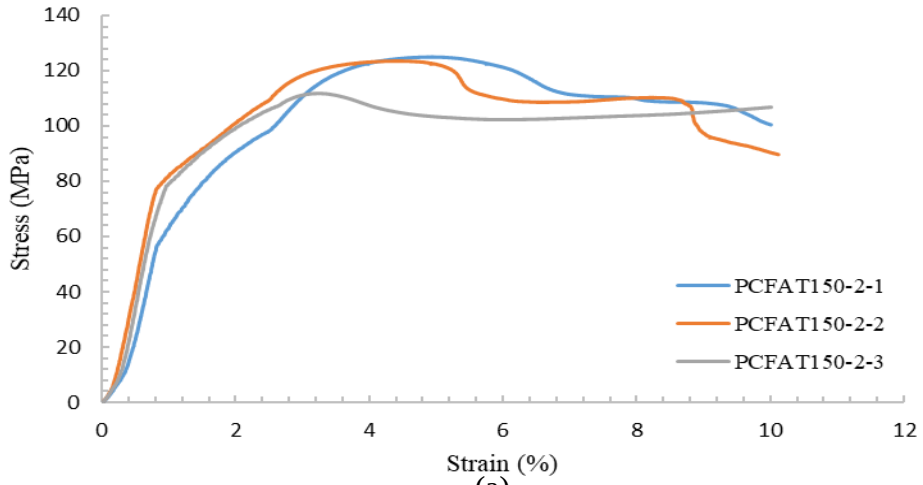

(a)

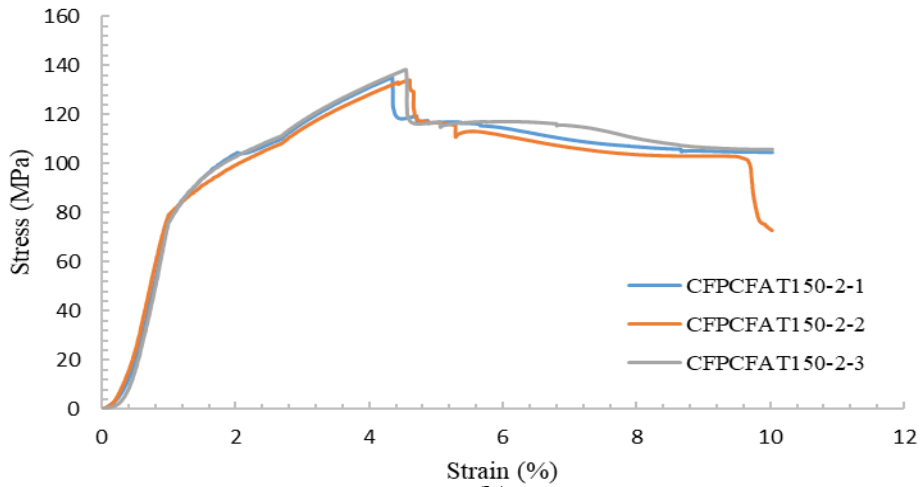

(b)

Figure 4.10 Stress-strain curves of (a) polymer concrete filled aluminum tube (PCFAT) and (b) carbon fiber wrapped PCFAT specimens having 50 mm diameter and 2 mm thickness

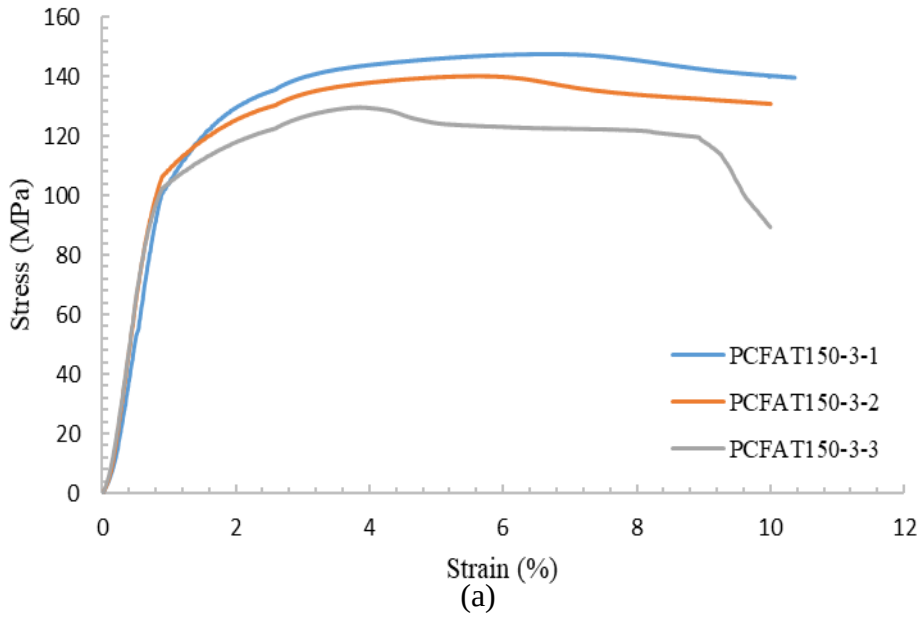

(a)

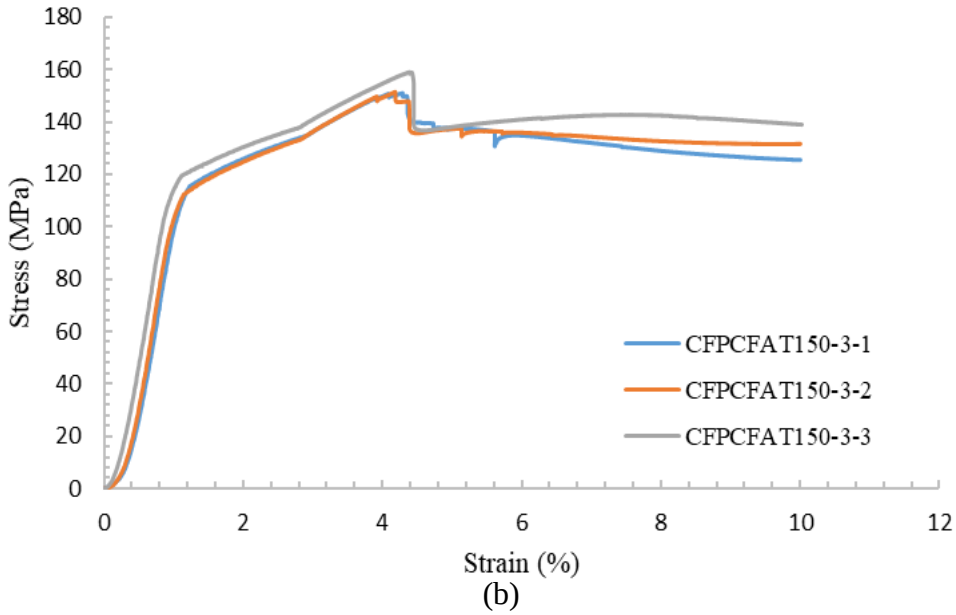

(b)

Figure 4.11 Stress-strain curves of (a) polymer concrete filled aluminum tube (PCFAT) and (b) carbon fiber wrapped PCFAT specimens having 50 mm diameter and 3 mm thickness

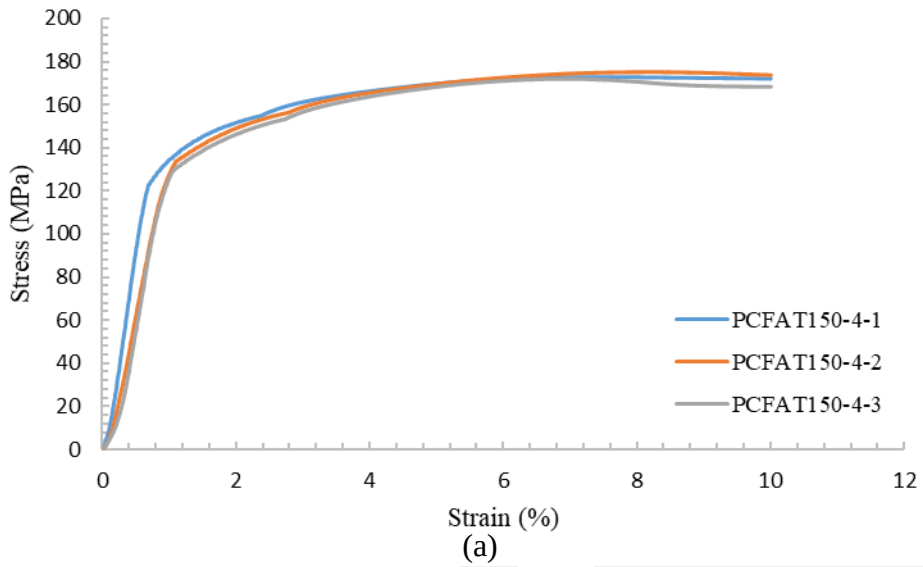

(a)

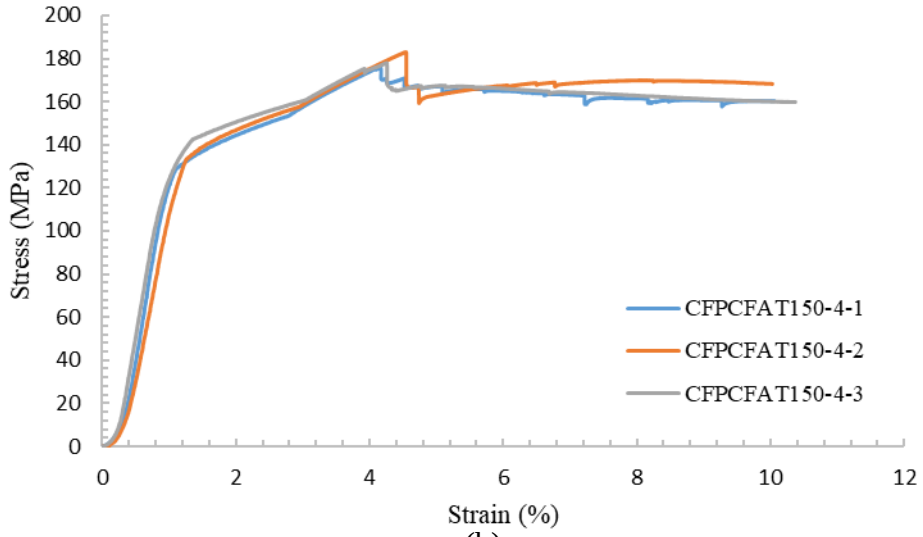

(b)

Figure 4.12 Stress-strain curves of (a) polymer concrete filled aluminum tube (PCFAT) and (b) carbon fiber wrapped PCFAT specimens having 50 mm diameter and 4 mm thickness

Fig. 4.10 shows stress-strain curves for PCFATs and CFPCFATs with 50 mm diameter and 2 mm thickness. An erratic behaviour was observed mostly in the plastic region of the curves which hardly overlap onto each other with increasing strain for PCFAT specimens. However, for CFPCFAT the deviation in the sample behaviour is not significant and the flow of the curves are more close to each other. We assume carbon fiber reinforcement helped to correct the erratic plastic deformation because of limited confinement effect of a thin tubular structure. In these diagrams, a sudden drop occurs after the peak load, which is caused by cracking and disconnection of the carbon fiber.

Moreover, with thicker specimens, this erratic behaviour in the plastic flow region was not observed, as shown in Figs. 4.11, and 4.12. We also determined that erratic behaviour in the plastic flow curve for thinner confinements become more significant with increasing length. We did not detect such vast oscillations for 120 mm long and 2 mm thick PCFAT specimens.

4.3.4.3 Compression test results for specimens with 60 mm diameter

The engineering stress-strain curves of the specimens confined with 60 mm diameter aluminum tubes having 2, 3 and 4 mm thickness and 180 mm length with and without carbon fiber wrap is presented in this section. Diameter to length ratio is kept constant at 1/3.

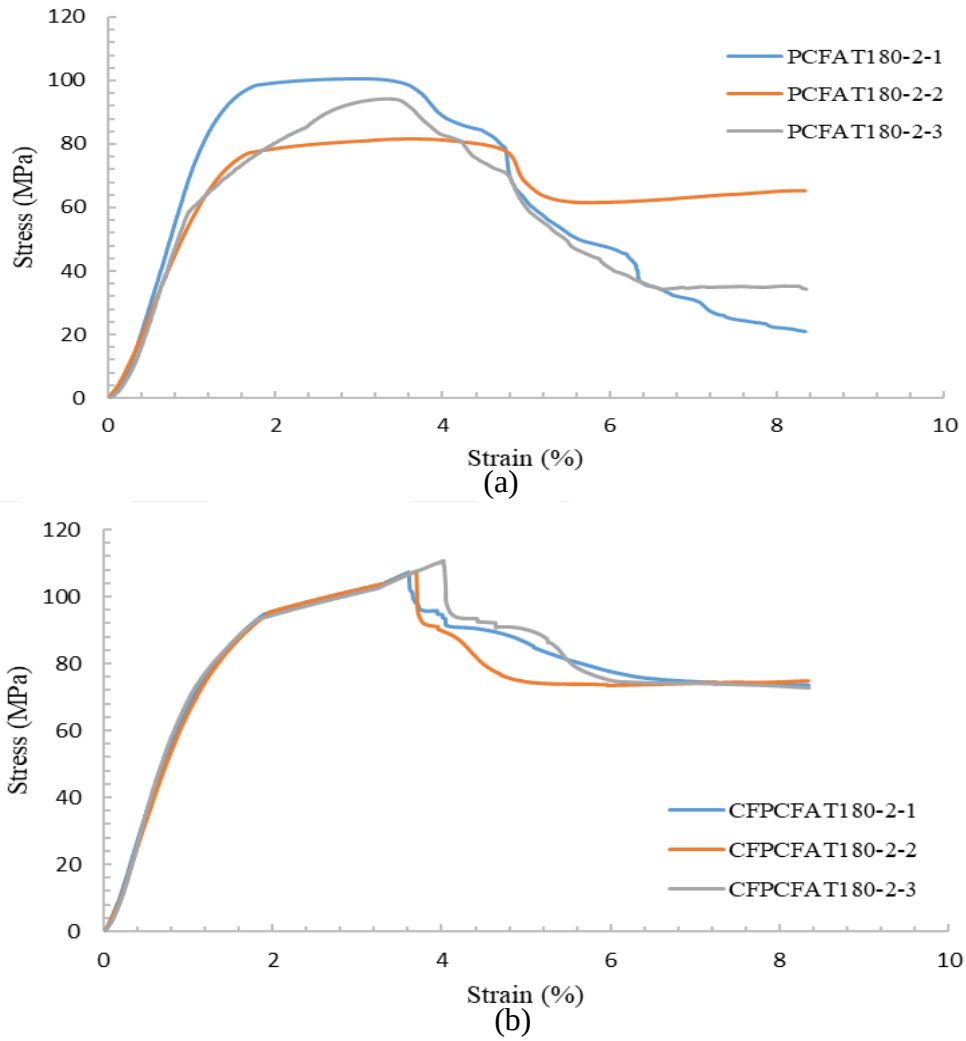

Figure 4.13 Stress-strain curves of (a) polymer concrete filled aluminum tube (PCFAT) and (b) carbon fiber wrapped PCFAT specimens having 60 mm diameter and 2 mm thickness

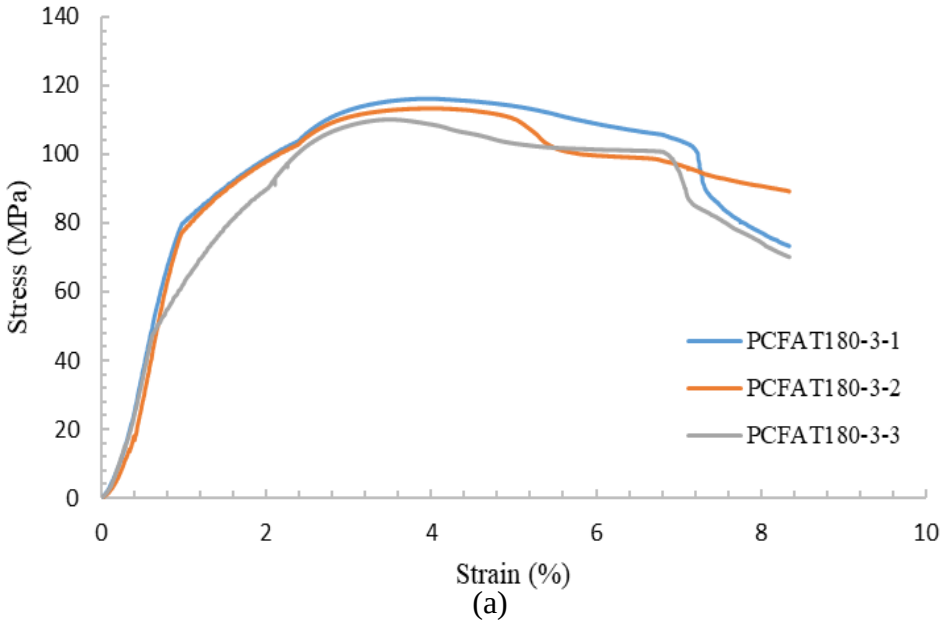

(a)

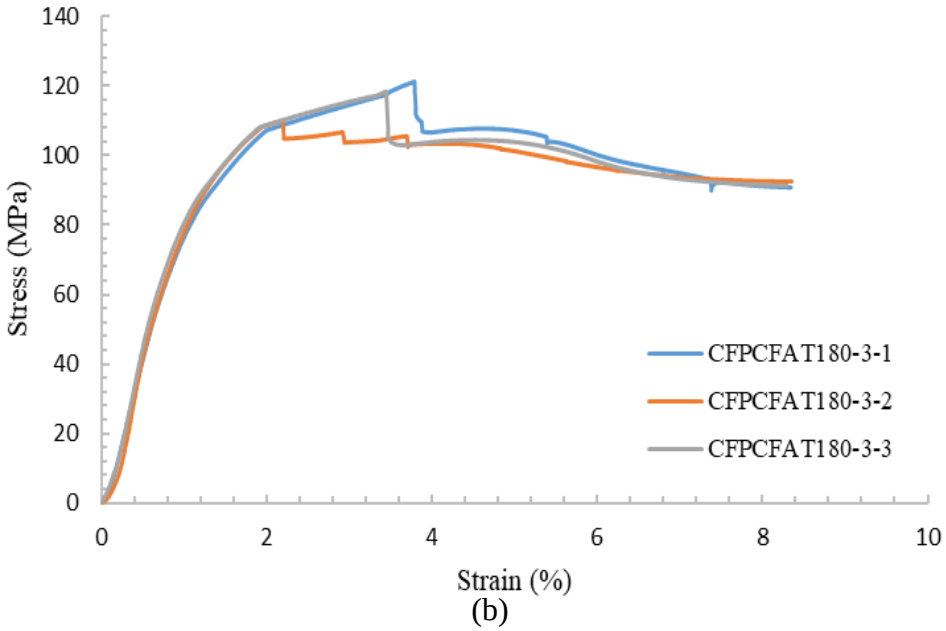

(b)

Figure 4.14 Stress-strain curves of (a) polymer concrete filled aluminum tube (PCFAT) and (b) carbon fiber wrapped PCFAT specimens having 60 mm diameter and 3 mm thickness

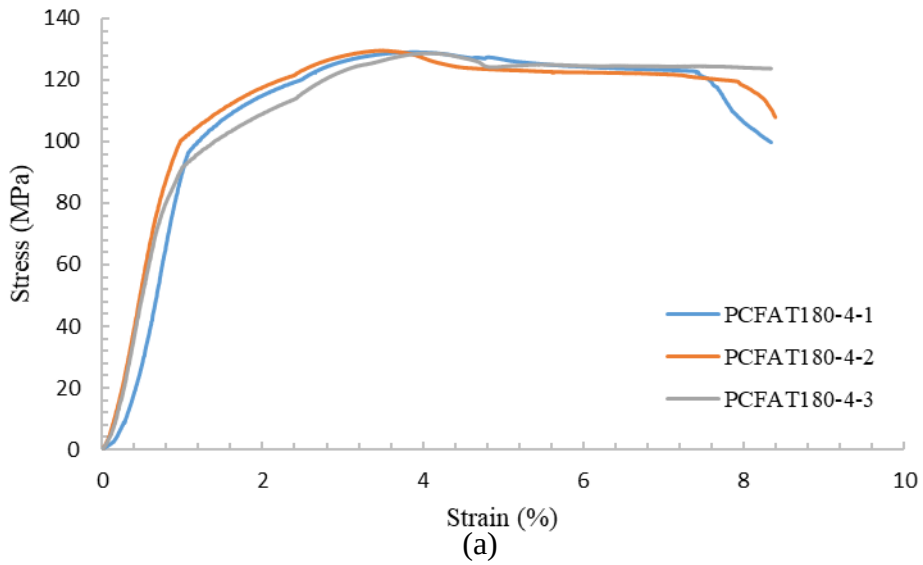

(a)

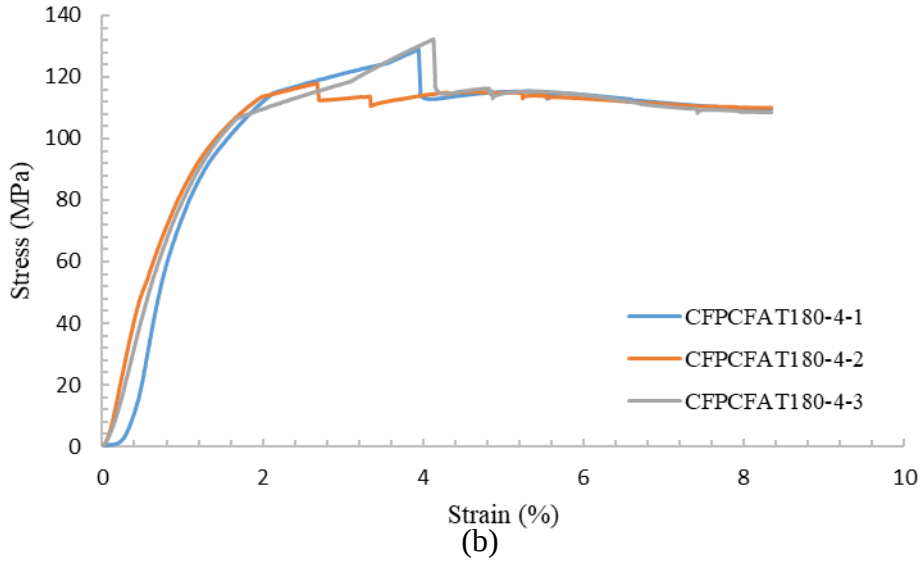

(b)

Figure 4.15 Stress-strain curves of (a) polymer concrete filled aluminum tube (PCFAT) and (b) carbon fiber wrapped PCFAT specimens having 60 mm diameter and 4 mm thickness

Fig. 4.13 shows typical stress-strain curves for PCFATs and CFPCFATs with 60 mm diameter and 2 mm thickness. We observe more erratic plastic deformation compared to 150 mm long tubular structures. When the thickness is increased from 2 mm to 3 and 4 mm, the ultimate load-carrying capacity increases and the flow curves approach each other and even overlap with 4mm thick tubular structures. Carbon fiber reinforcement for 2 mm thick samples is effective until the peak stress where carbon fibers broke apart. Then, erratic plastic flow curves appear since the only confinement left was the aluminum tubes which are not significantly effective at 2 mm thickness

level. This proves that carbon fiber reinforcement is very effective to attain a more uniform plastic deformation for thin walled Aluminum tubes. Also, the post-peak region of the curve in the case of polymer concrete core significantly lesser than that of PCFAT or CFPCFAT specimens because the concrete is a brittle material by nature and the presence of the ductile aluminum as confinement in the PCFAT and CFPCFAT specimens is responsible for the increased ductility and toughness. This, in turn, leads to a gradual drop and more stability in the shape of stress-strain curves after the peak point load for both PCFATs and CFPCFATs, as its evident in Figs 4.14 and 4.15.

4.3.4.4 Compression test results for specimens with 70 mm diameter

The engineering stress-strain curves of the specimens confined with 70 mm diameter aluminum tubes having 2, 3 and 4 mm thickness and 210 mm length with and without carbon fiber wrap is presented in this section. Diameter to length ratio is kept constant at 1/3.

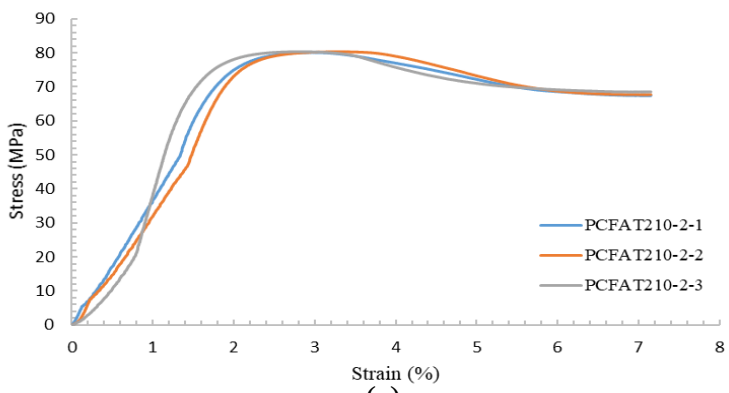

(a)

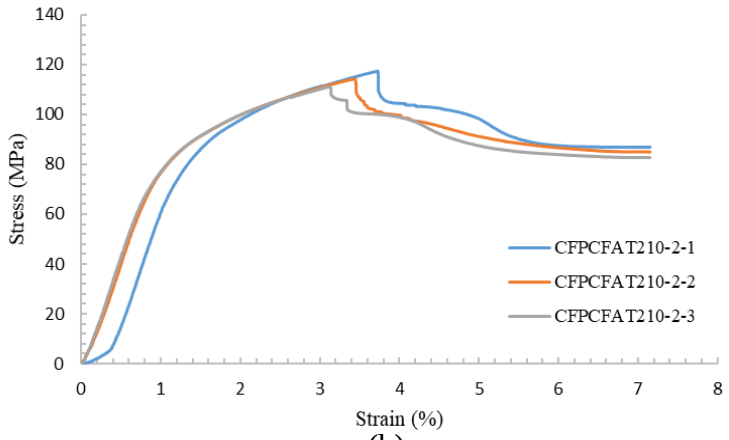

(b)

Figure 4.16 Stress-strain curves of (a) polymer concrete filled aluminum tube (PCFAT) and (b) carbon fiber wrapped PCFAT specimens having 70 mm diameter and 2 mm thickness

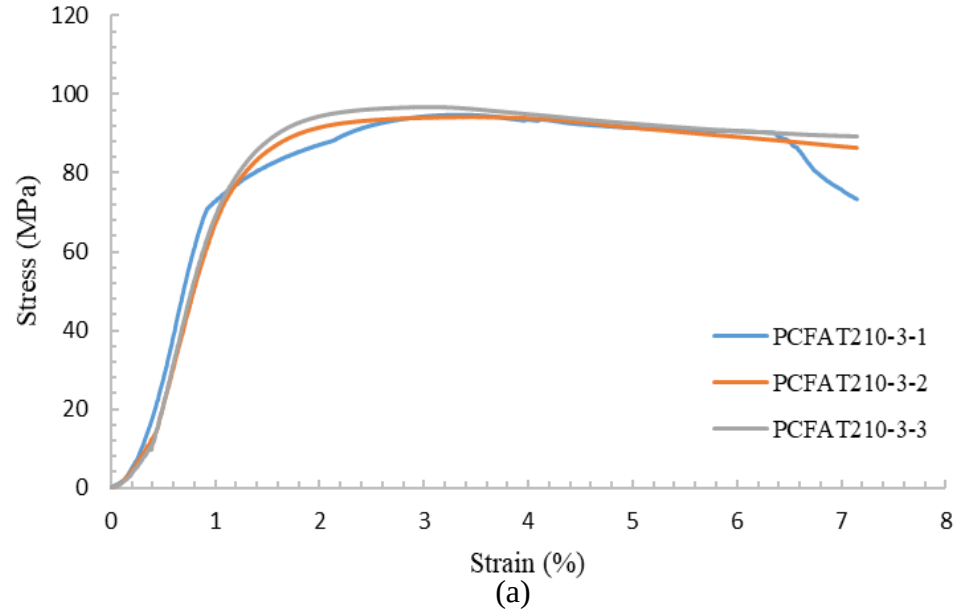

(a)

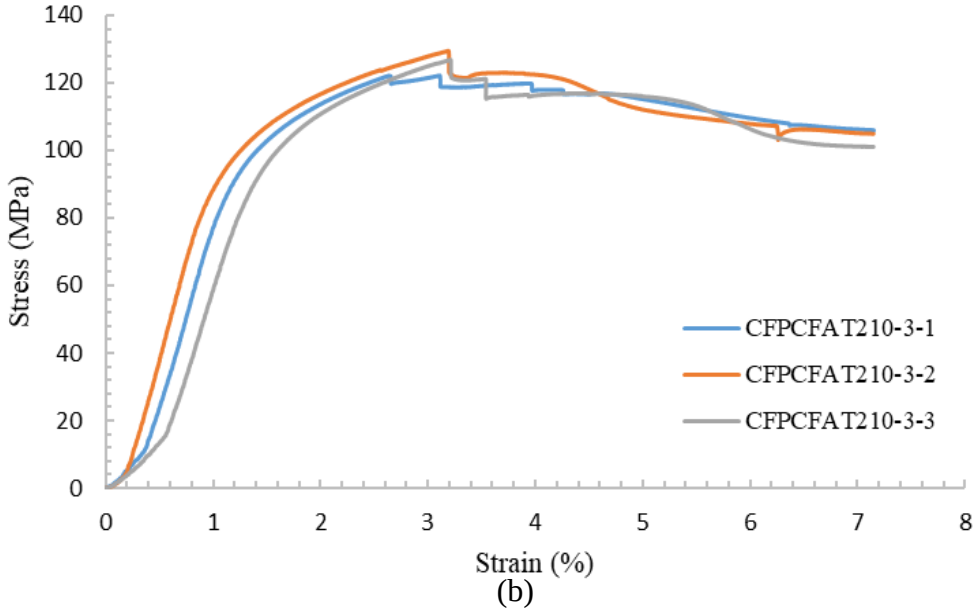

(b)

Figure 4.17 Stress-strain curves of (a) polymer concrete filled aluminum tube (PCFAT) and (b) carbon fiber wrapped PCFAT specimens having 70 mm diameter and 3 mm thickness

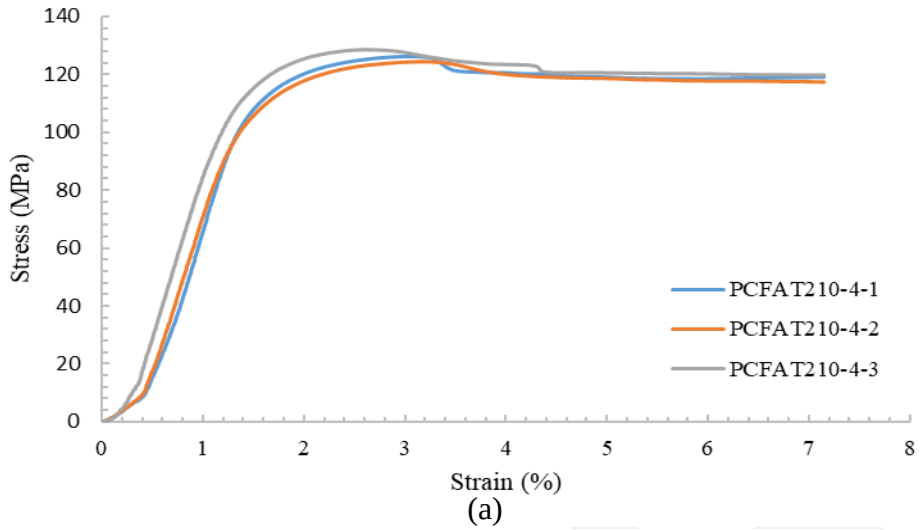

(a)

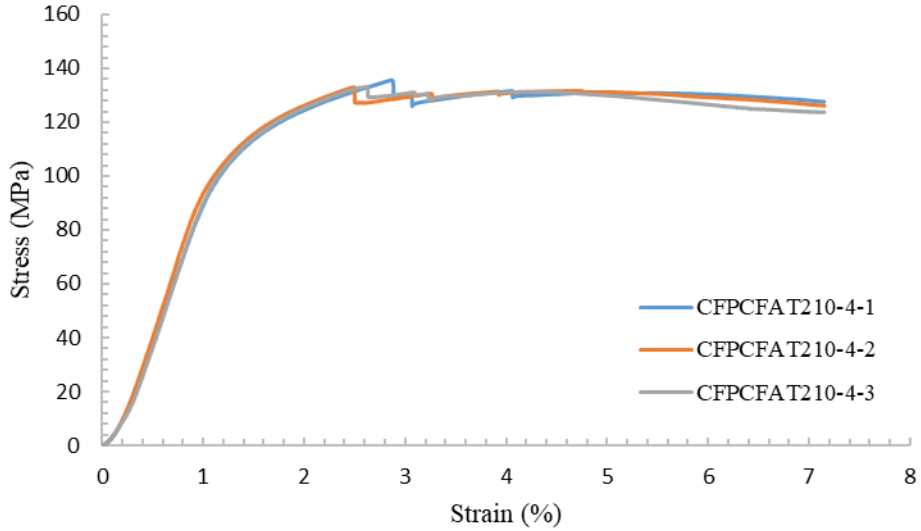

(b)

Figure 4.18 Stress-strain curves of (a) polymer concrete filled aluminum tube (PCFAT) and (b) carbon fiber wrapped PCFAT specimens having 70 mm diameter and 4 mm thickness

Fig. 4.16 shows stress-strain curves for PCFATs and CFPCFATs with 70 mm diameter and 2 mm thickness. The amount of strength these specimens can handle is far less than the previous samples, lower than 100 MPa. Even though the diameter to length ratio is constant, we assume that length plays a crucial role on strength after some threshold value. One should expect an erratic behaviour in the plastic deformation region of PCFAT samples since the length is increased further, yet plastic flow curves are approached each other. In addition, a noticeable change in the shape of the stress-strain curves for CFPCFAT specimens are observed compared with the PCFAT specimens. It is also seen from the figures that the ultimate stress is higher in

CFPCFATs compared to PCFATS. It should be noted that the sudden drop in the stress after the peak point for CFPCAT becomes less visible with the increase in thickness, as shown in Figs. 4.17 and 4.18. Instead, a gradual cracking of the carbon fibers occur.

4.3.5 Failure modes

4.3.5.1 HCAT specimens

In HCAT specimens, the failure mode of the aluminum tube was mainly outward buckling around the circumference. This local buckling mode near the tube end, widely known as the elephant's leg buckling mode, is typically found in aluminum tubes whose diameter-to-thickness ratio is relatively small. Fig. 4.19 shows the failure mode development of the HCAT-150 specimens (D=50 mm) with 2, 3, and 4 mm in thickness, respectively. However, when diameter-to-thickness decreases, we notice outward and inward buckling in the sample as it happened in the HCAT-180-2-1 specimen (D=60 mm), as shown in Fig. 4.20.

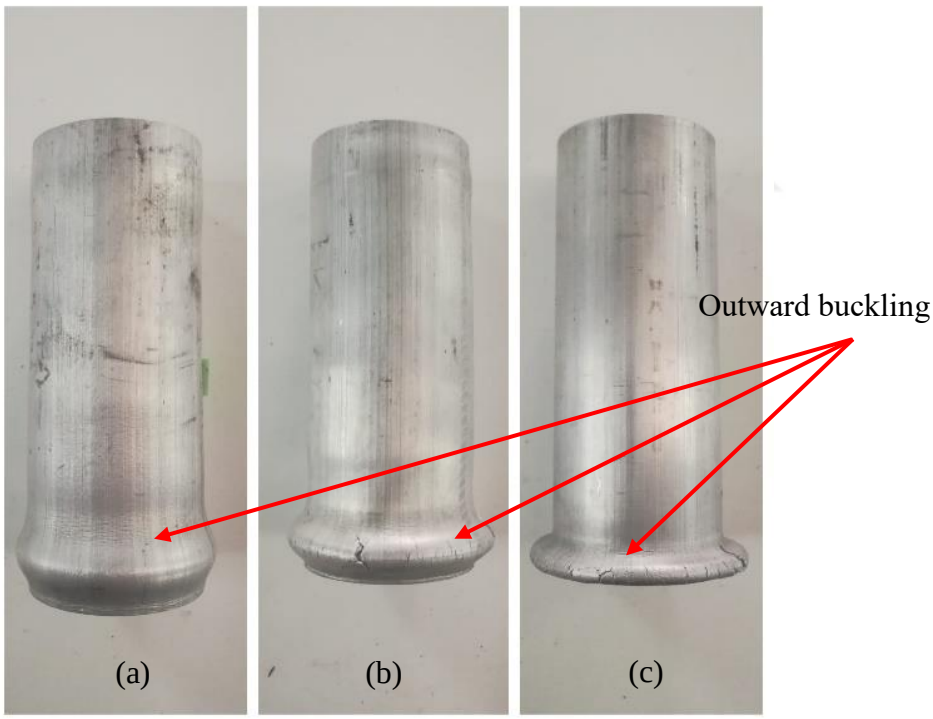

Figure 4.19 Failure mode of HCAT-150 specimens (D=50 mm) with (a) 4 mm (b) 3 mm (c) 2 mm thickness

Figure 4.20 Failure mode of HCAT-180-2-1 specimen (D=60 mm)

4.3.5.2 PCFAT specimens

For PCFAT specimens, the polymer concrete core prevents the aluminum from inward buckling and increases the element's stability, stiffness, and capacity. On the other hand, the aluminum tube acts as a longitudinal and transverse reinforcement to prevent polymer concrete spalling and provides the polymer concrete confinement, which puts it under a triaxial stress state. Generally, the modes of failure are primarily characterized by polymer concrete crushing followed by a local buckling in aluminum tubes. The aluminum's local buckling is closer to the specimen ends due to the shear failure in the polymer concrete after crushing. Fig. 4.21 shows the failure mode of the PCFAT-120 specimens (D=40 mm) with 2, 3, and 4 mm in thickness, respectively.

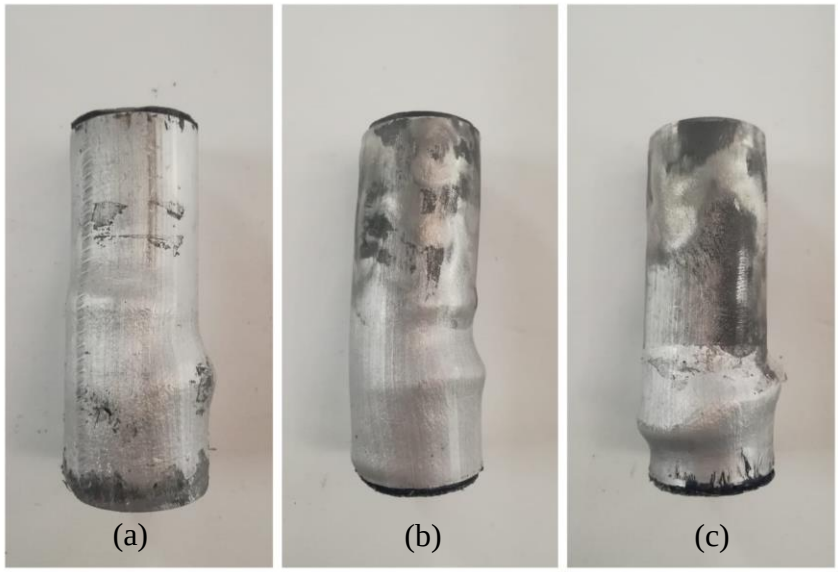

Figure 4.21 Failure mode of PCFAT-120 specimens (D=40 mm) with (a) 4 mm (b) 3 mm (c) 2 mm thickness

4.3.5.3 CFPCFAT specimens

In CFPCFAT specimens, the filled aluminum tubes experienced continuous dilation in the lower end region. Localized outward buckling of the aluminum tube near the tube ends at large axial shortenings values is also observed. All specimens failed by rupture of the carbon fiber reinforced polymer (CFRP) in the mid-height region to the lower end due to the polymer concrete's lateral expansion below it is center. The typical failure modes are shown in Fig. 4.22. The volume expansion of the polymer concrete and the aluminum tube's local buckling in CFPCFAT specimens was not cancelled but rather delayed.

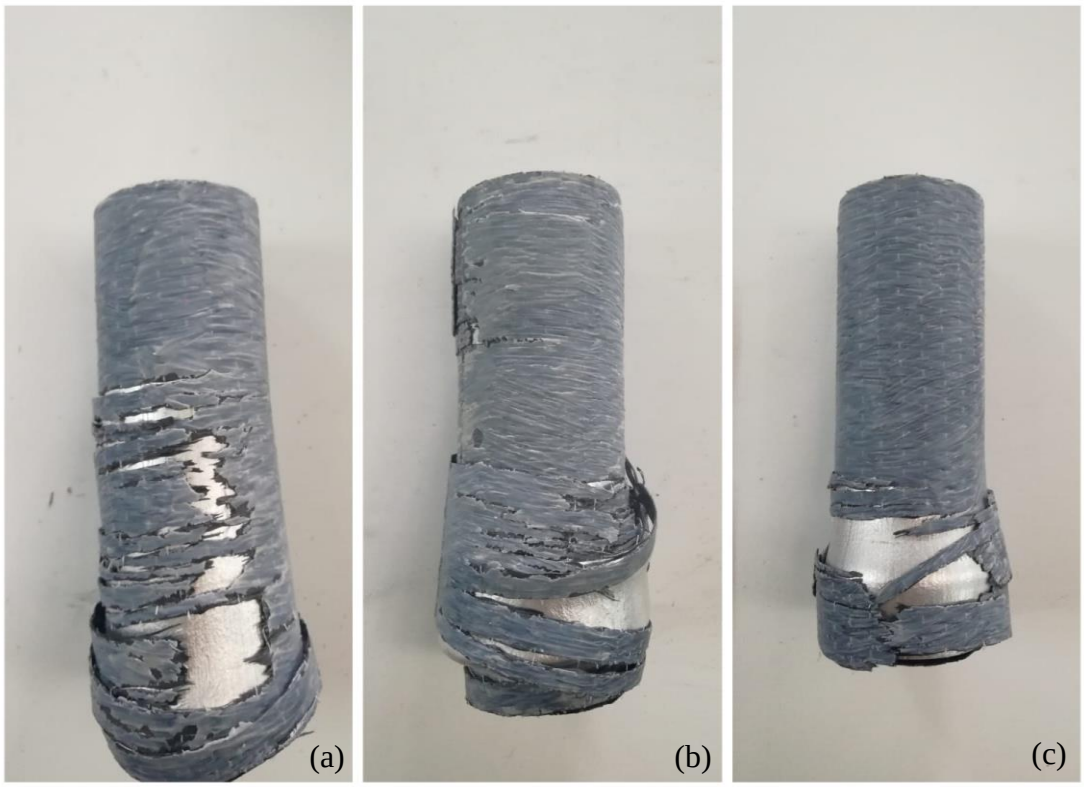

Figure 4.22 Failure mode of CFPCAT -150 specimens (D=50 mm) with (a) 2 mm (b) 3 mm (c) 4 mm thickness

4.3.6 Axial stiffness

The general definition for stiffness, K, is a measure of the resistance of a member to deformation. In CFT's, the axial stiffness is defined by Park, Yeom et al.[42] as the ultimate capacity P_u over displacement at that load (δ_{y1}) as seen in Eq.4.1.

$$K = \frac{P_u}{\delta_{y1}} \tag{4.1}$$

The stiffness results for PCFAT are shown in Fig. 4.23 and Table 4.6. The values depend on the cross-sectional area and the thickness. When the cross-sectional area and thickness increases, the stiffness values are increased. For CFPCFAT specimens, the results showed that the CFRP reinforcement reduces unevenness caused by thickness differences and provides a moderate increase in stiffness, as shown in Fig. 4.24 and Table 4.7 .

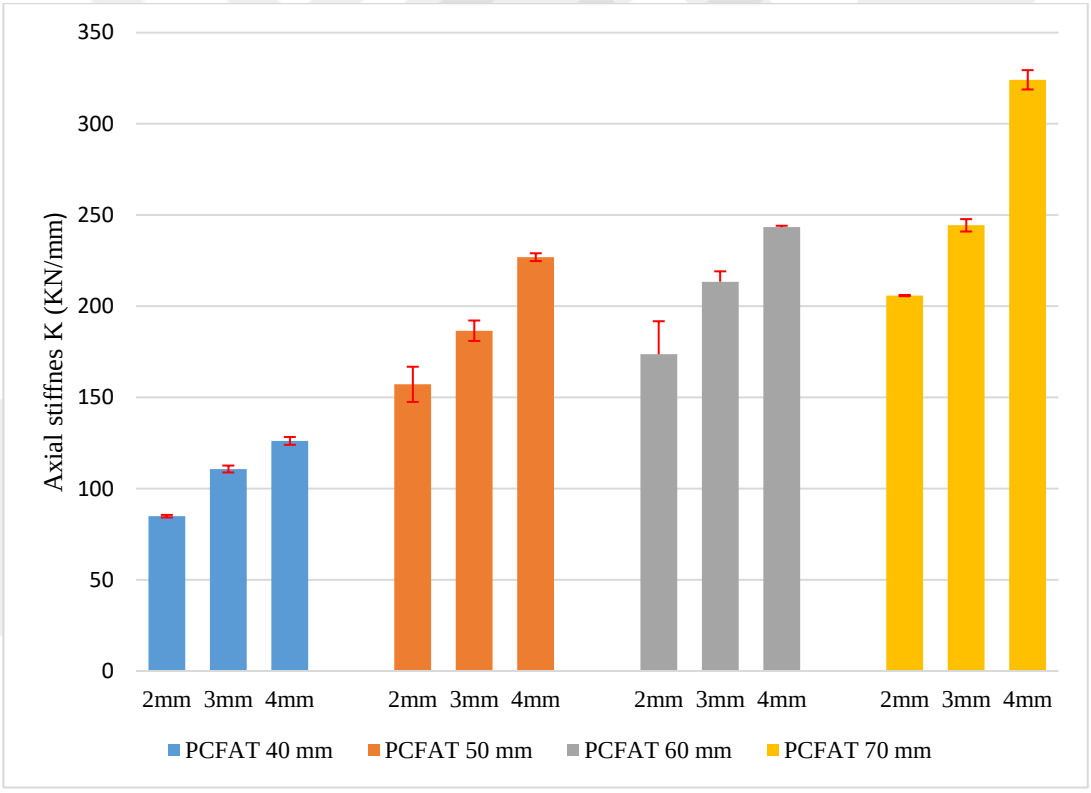

Figure 4.23 Axial stuffiness of PCFAT specimens

Table 4.6 Axial stuffiness of PCFAT specimens

Specimen	Diameter, D (mm)	Thickness, t (mm)	Ultimate capacity P_u (KN)	Axial stiffness K (KN)
PCFAT120-2-1	40	2		
PCFAT120-2-2	40	2	127.31	84.871
PCFAT120-2-3	40	2		
PCFAT120-3-1	40	3		
PCFAT120-3-2	40	3	166.12	110.743
PCFAT120-3-3	40	3		
PCFAT120-4-1	40	4		
PCFAT120-4-2	40	4	189.22	126.145
PCFAT120-4-3	40	4		
PCFAT150-2-1	50	2		
PCFAT150-2-2	50	2	235.75	157.163
PCFAT150-2-3	50	2		
PCFAT150-3-1	50	3		
PCFAT150-3-2	50	3	279.78	186.549
PCFAT150-3-3	50	3		
PCFAT150-4-1	50	4		
PCFAT150-4-2	50	4	340.31	226.871
PCFAT150-4-3	50	4		
PCFAT180-2-1	60	2		
PCFAT180-2-2	60	2	260.43	173.618
PCFAT180-2-3	60	2		
PCFAT180-3-1	60	3		
PCFAT180-3-2	60	3	320.12	213.414
PCFAT180-3-3	60	3		
PCFAT180-4-1	60	4		
PCFAT180-4-2	60	4	364.93	243.285
PCFAT180-4-3	60	4		
PCFAT210-2-1	70	2		
PCFAT210-2-2	70	2	308.74	205.823
PCFAT210-2-3	70	2		
PCFAT210-3-1	70	3		
PCFAT210-3-2	70	3	366.50	244.335
PCFAT210-3-3	70	3		
PCFAT210-4-1	70	4		
PCFAT210-4-2	70	4	486.15	324.102
PCFAT210-4-3	70	4		

Table 4.7 Axial stuffiness of CFPCFAT specimens

Specimen	Diameter, D (mm)	Thickness, t (mm)	Ultimate capacity P_u (KN)	Axial stiffness K (KN)
CFPCAT120-2-1	40	2		
CFPCAT120-2-2	40	2	183.30	119.563
CFPCAT120-2-3	40	2		
CFPCAT120-3-1	40	3		
CFPCAT120-3-2	40	3	213.84	140.263
CFPCAT120-3-3	40	3		
CFPCAT120-4-1	40	4		
CFPCAT120-4-2	40	4	227.81	148.131
CFPCAT120-4-3	40	4		
CFPCAT150-2-1	50	2		
CFPCAT150-2-2	50	2	266.52	177.681
CFPCAT150-2-3	50	2		
CFPCAT150-3-1	50	3		
CFPCAT150-3-2	50	3	302.00	201.335
CFPCAT150-3-3	50	3		
CFPCAT150-4-1	50	4		
CFPCAT150-4-2	50	4	351.20	234.134
CFPCAT150-4-3	50	4		
CFPCAT180-2-1	60	2		
CFPCAT180-2-2	60	2	306.79	204.5299
CFPCAT180-2-3	60	2		
CFPCAT180-3-1	60	3		
CFPCAT180-3-2	60	3	329.52	219.676
CFPCAT180-3-3	60	3		
CFPCAT180-4-1	60	4		
CFPCAT180-4-2	60	4	367.54	238.206
CFPCAT180-4-3	60	4		
CFPCAT210-2-1	70	2		
CFPCAT210-2-2	70	2	439.48	292.9841
CFPCAT210-2-3	70	2		
CFPCAT210-3-1	70	3		
CFPCAT210-3-2	70	3	485.19	323.459
CFPCAT210-3-3	70	3		
CFPCAT210-4-1	70	4		
CFPCAT210-4-2	70	4	515.23	343.485
CFPCAT210-4-3	70	4		

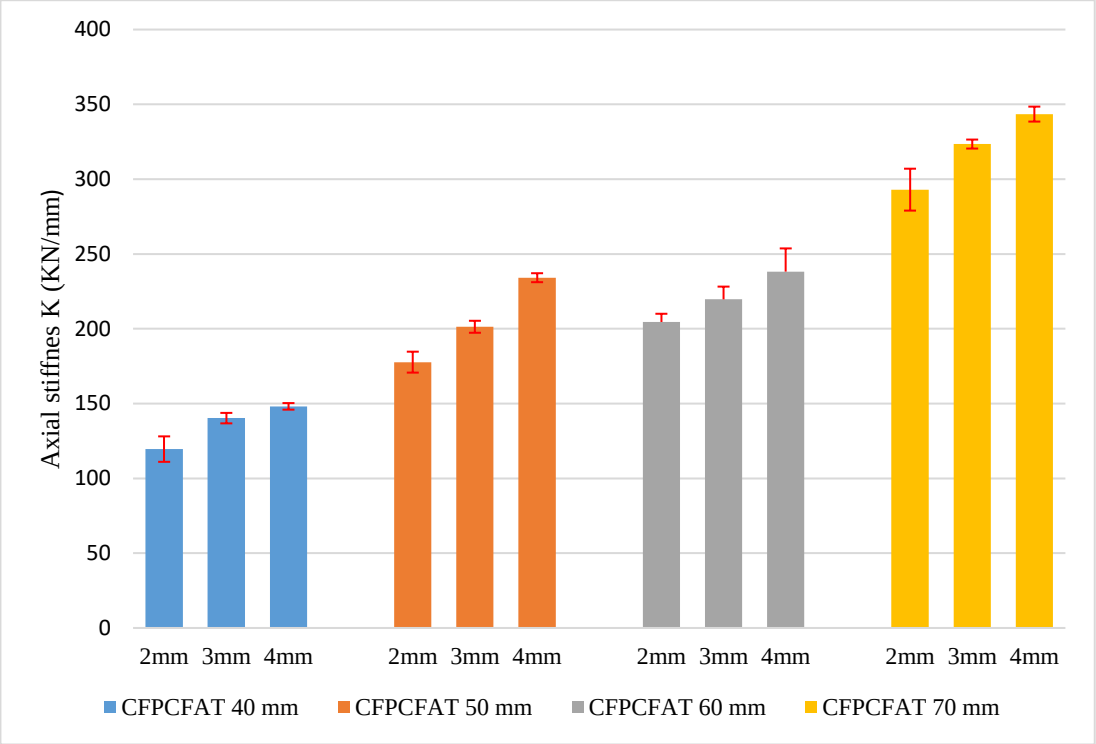

Figure 4.24 Axial stuffiness of CFPCFAT specimens

4.3.7 Analytical models for predicting the load bearing capacity

Two analytical models for the prediction of axial load capacity of both PCFAT and CFPCFATs are used in this study. The first model is the model proposed by the Sakino [43], developed to determine the ultimate axial load capacity of concrete-filled steel columns. The second model is developed by Tang et al. [18], which was used to model FRP confined concrete filled stainless steel tubes under axial compression. In this part, these models are used with the material properties of PC and aluminum to predict the axial capacity of the PCFAT and CFPCFATs analytically and compare it with the experimental results.

4.3.7.1 Model for the PCFAT tubes

The maximum axial loads (N_{exp}) obtained from experiments of PCFAT tubes are summarized in Table 4.8. The non-dimensional maximum axial loads in the form of N_{exp}/N_o are also given in the table, where N_o is the nominal squash load given by

$$N_O = A_{al}\,\sigma_{scy} + A_C\,\gamma_u\,f_c' \tag{4.2}$$

In this equation, A_{al} and A_c are the cross-sectional area of aluminum tube and filled polymer concrete, respectively; and f_c' is the compressive strength of filled polymer concrete (=51.88 MPa). In addition, γ_u is a strength reduction factor calculated by the following formula [43].

$$\gamma_u = 1.67\, D_c^{-0.112} \tag{4.3}$$

Here, D_c is the diameter of the polymer concrete specimen. The average compressive yield strength values σ_{scy} are obtained through experiments are aslo given in Table 4.8, and it is used to evaluate N_O in Eq. (4.2). σ_{scy} values are determined using 0.2% offset yield strength method as shown in Fig.4.25 for HCAT120-2-1specimen. It should be noted that the stress-strain diagram for HCATs are used in the determination of σ_{scy}.

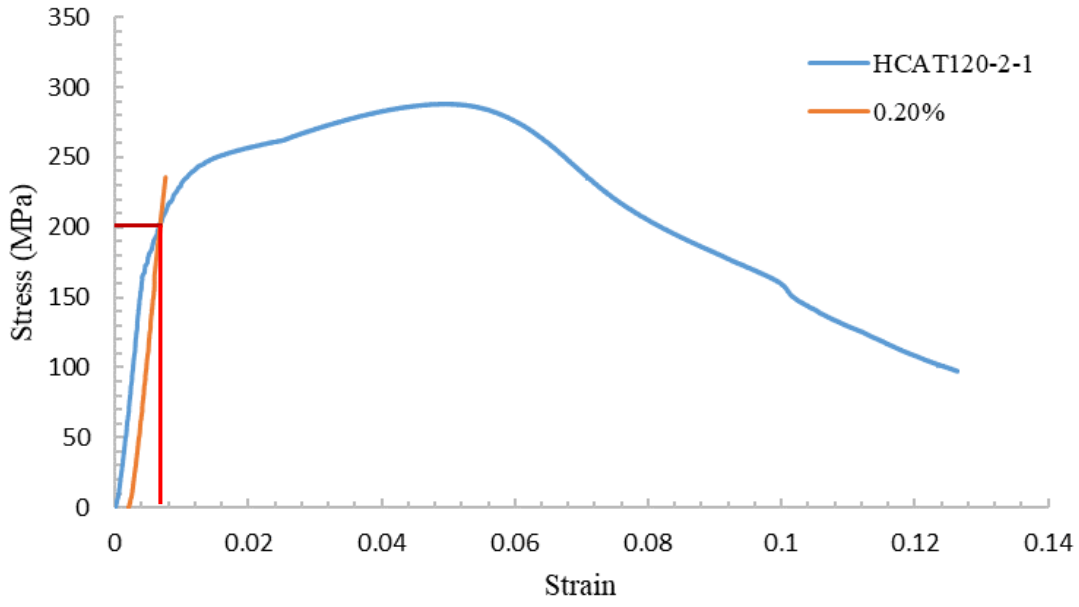

Figure 4.25 0.2% offset yield strength of the HCAT120-2-1 specimen

Table 4.8 Experimental variables and test results

Specimen	A_{al} (mm)	A_c (mm)	σ_{scy} (MPa)	N_o	N_{exp}(kN)	N_{exp} / N_o
PCFAT120-2-1 PCFAT120-2-2 PCFAT120-2-3	238.64	1017.36	229.097	111.545	127.308	1.141
PCFAT120-3-1 PCFAT120-3-2 PCFAT120-3-3	348.54	907.46	230.607	131.105	166.115	1.267
PCFAT120-4-1 PCFAT120-4-2 PCFAT120-4-3	452.16	803.84	227.637	147.865	189.219	1.280
PCFAT150-2-1 PCFAT150-2-2 PCFAT150-2-3	301.44	1661.06	331.843	192.888	235.745	1.222
PCFAT150-3-1 PCFAT150-3-2 PCFAT150-3-3	442.74	1519.76	328.427	230.366	279.784	1.215
PCFAT150-4-1 PCFAT150-4-2 PCFAT150-4-3	577.76	1384.74	333.743	270.234	340.307	1.259
PCFAT180-2-1 PCFAT180-2-2 PCFAT180-2-3	364.24	2461.76	193.777	208.200	260.428	1.251
PCFAT180-3-1 PCFAT180-3-2 PCFAT180-3-3	536.94	2289.06	276.400	276.375	320.122	1.158
PCFAT180-4-1 PCFAT180-4-2 PCFAT180-4-3	703.36	2122.64	279.223	315.056	364.929	1.158
PCFAT210-2-1 PCFAT210-2-2 PCFAT210-2-3	427.04	3419.46	312.357	324.545	308.736	0.951
PCFAT210-3-1 PCFAT210-3-2 PCFAT210-3-3	631.14	3215.36	319.703	381.524	366.503	0.961
PCFAT210-4-1 PCFAT210-4-2 PCFAT210-4-3	828.96	3017.54	321.980	435.597	486.154	1.116

As shown in Table 4.8, the maximum axial load N_{exp} is greater then the nominal squash load N_O in almost all of the PCFAT tubes. The main reason for this augmentation of axial load capacity is attributed to the confinement effect of the aluminum tube on the polymer concrete.

On the other hand, the axial yield strength of aluminum tubes (N_{SO}) can be obtained by.

$$N_{SO} = A_{al}\, \sigma_{sy} \tag{4.4}$$

where A_{al} is the cross-sectional area of aluminum tube and σ_{sy} is the mean tensile yield stress of aluminum tube obtained from the coupon test. A value of 244.433 MPa is used in this study, which is the average of the coupon test results.

Since the Poisson's ratio for concrete is lower than that for aluminum, when the PCFAT tubes are subjected to axial load in the early stages of loading, a separation between the aluminum tube and the polymer concrete core develops. The longitudinal strain reaches a critical level as the load increases, and the lateral deformation of the polymer concrete catches up to the aluminum tube. The aluminum tube develops a tensile hoop stress as the load increases, and the polymer concrete core experiences tri-axial compression. The axial compressive load capacity increases as a result of this phenomenon. The equation for axial compressive load capacity is obtained by a series of calculations.

The confined polymer concrete strength is calculated by

$$\sigma_{ccB} = \gamma_u\, f_c' + k\sigma_r \tag{4.5}$$

where, σ_{ccB} is the strength of confined polymer concrete, γ_u is a strength reduction factor, f_c' is the compressive strength of filled polymer concrete, k is confinement coefficient (k=4.1) according to Richart et al.[42], and σ_r is the confining stress (lateral pressure).

The stresses in the aluminum tubes at the ultimate load can be obtained by

$$\sigma_{s\theta} = \alpha_u\, \sigma_{sy} \tag{4.6}$$

$$\sigma_{sz} = \beta_{uc}\, \sigma_{sy} \tag{4.7}$$

In this equation, $\sigma_{s\theta}$ and σ_{sz} are the hoop and axial stresses, respectively. α_u and β_{uc} are coefficients independent of the material properties and determined based on experimental results.

The relation between the lateral pressure and the hoop stress is obtained by

$$\sigma_r = -\frac{2t}{D-2t}\sigma_{s\theta} \tag{4.8}$$

Here, σ_r is the lateral pressure and $\sigma_{s\theta}$ is the hoop stress, and D, t are the diameter and thickness of the aluminum tube, respectively.

The difference between the nominal squash load N_O and the ultimate strength N_u is influenced by the confinement effect. In order to determine the confinement effect on polymer concrete strength, the ultimate strength N_u is calculated as

$$N_u = A_{al}\,\sigma_{sz} + A_C\,\sigma_{ccB} \tag{4.9}$$

The value of the normalized axial compressive load capacity can be given as

$$\lambda = \beta_{uc} - 1 - \frac{D-2t}{2(D-2t)}k\alpha_u \tag{4.10}$$

where λ is a linear function of the parameter N_{SO}/N_o. The value of λ is determined by a regression analysis based on experimental data. The relation between stress coefficients α_u and β_{uc} is obtained from the assumption that stresses in the aluminum tube at the ultimate state causes yielding. The relation between α_u and β_{uc} can be written using von Mises yield stress and Eqns. 4.6 and 4.7 as

$${\alpha_u}^2 - \alpha_u\beta_{uc} + {\beta_{uc}}^2 = 1 \tag{4.11}$$

Once the value of λ are determined and fixed, the values of α_u and β_{uc} are determined by solving Eqns. 4.10 and 4.11 simultaneously.

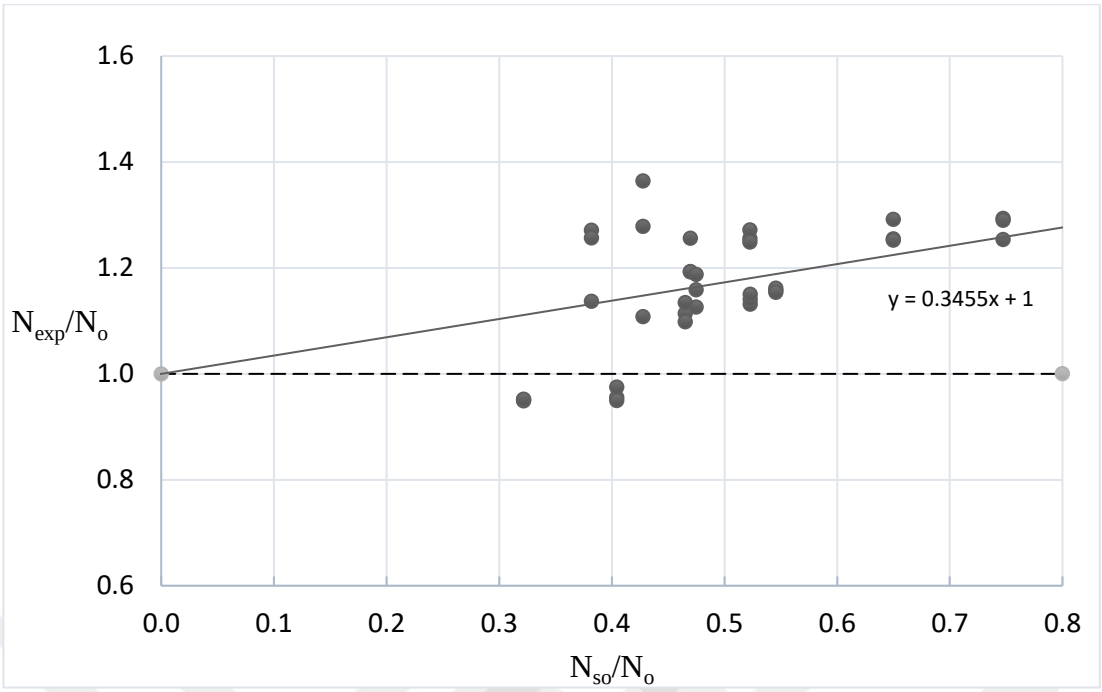

Figure 4.26 Experimental axial compressive load capacities of polymer concrete-filled aluminum tubes

Fig 4.26 shows the relationships between experimental axial load capacity N_{exp} of the PCFATs and yield load of the aluminum tubes N_{so}. The slope of the line is λ and it is determined as 0.3455. Since the value of λ is known; using Eqns. 4.10 and 4.11, the value of coefficients α_u and β_{uc} are determined for the PCFAT tubes. Once these coefficients are calculated, we can find the stresses and axial load capacity of the assemblies.

In order to verify the effectiveness of the design equations of the load-carrying capacity of the polymer concrete-filled aluminum tubes under axial compression, comparisons are made between the calculated and the experimental values for the PCFATs. A mean ratio of 1.059 for N_{exp} / N_u and a standard deviation of 0.120 are obtained. Table 4.9 shows the experimental and the calculated results, while Fig. 4.27 compares the experimental and calculated results of PCFATs.

Table 4.9 Calculated parameters and test results of PCFATs

Specimen	αu	βuc	$\sigma_{s\theta}$ (MPa)	σ_{sz} (MPa)	σ_r (MPa)	σ_{ccB} (MPa)	N_u (kN)	N_{exp} (kN)	N_{exp} / N_u
PCFAT120-2-1									
PCFAT120-2-2	-0.26	0.85	-62.81	206.90	6.98	84.52	135.36	127.31	0.94
PCFAT120-2-3									
PCFAT120-3-1									
PCFAT120-3-2	-0.27	0.84	-65.91	204.72	11.63	103.59	165.36	166.12	1.00
PCFAT120-3-3									
PCFAT120-4-1									
PCFAT120-4-2	-0.28	0.83	-69.58	202.10	17.39	127.22	193.65	189.22	0.98
PCFAT120-4-3									
PCFAT150-2-1									
PCFAT150-2-2	-0.25	0.85	-61.70	207.67	5.37	77.90	192.00	235.75	1.23
PCFAT150-2-3									
PCFAT150-3-1									
PCFAT150-3-2	-0.26	0.84	-63.99	206.07	8.73	91.68	230.57	279.78	1.21
PCFAT150-3-3									
PCFAT150-4-1									
PCFAT150-4-2	-0.27	0.84	-66.60	204.23	12.69	107.91	267.43	340.31	1.27
PCFAT150-4-3									
PCFAT180-2-1									
PCFAT180-2-2	-0.25	0.85	-60.99	208.16	4.36	73.76	257.41	260.43	1.01
PCFAT180-2-3									
PCFAT180-3-1									
PCFAT180-3-2	-0.26	0.85	-62.81	206.90	6.98	84.52	304.56	320.12	1.05
PCFAT180-3-3									
PCFAT180-4-1									
PCFAT180-4-2	-0.27	0.84	-64.82	205.49	9.97	96.79	349.99	364.93	1.04
PCFAT180-4-3									
PCFAT210-2-1									
PCFAT210-2-2	-0.25	0.85	-60.50	208.50	3.67	70.94	331.60	308.74	0.93
PCFAT210-2-3									
PCFAT210-3-1									
PCFAT210-3-2	-0.25	0.85	-62.01	207.46	5.81	79.74	387.32	366.50	0.95
PCFAT210-3-3									
PCFAT210-4-1									
PCFAT210-4-2	-0.26	0.84	-63.65	206.31	8.21	89.57	441.32	486.15	1.10
PCFAT210-4-3									

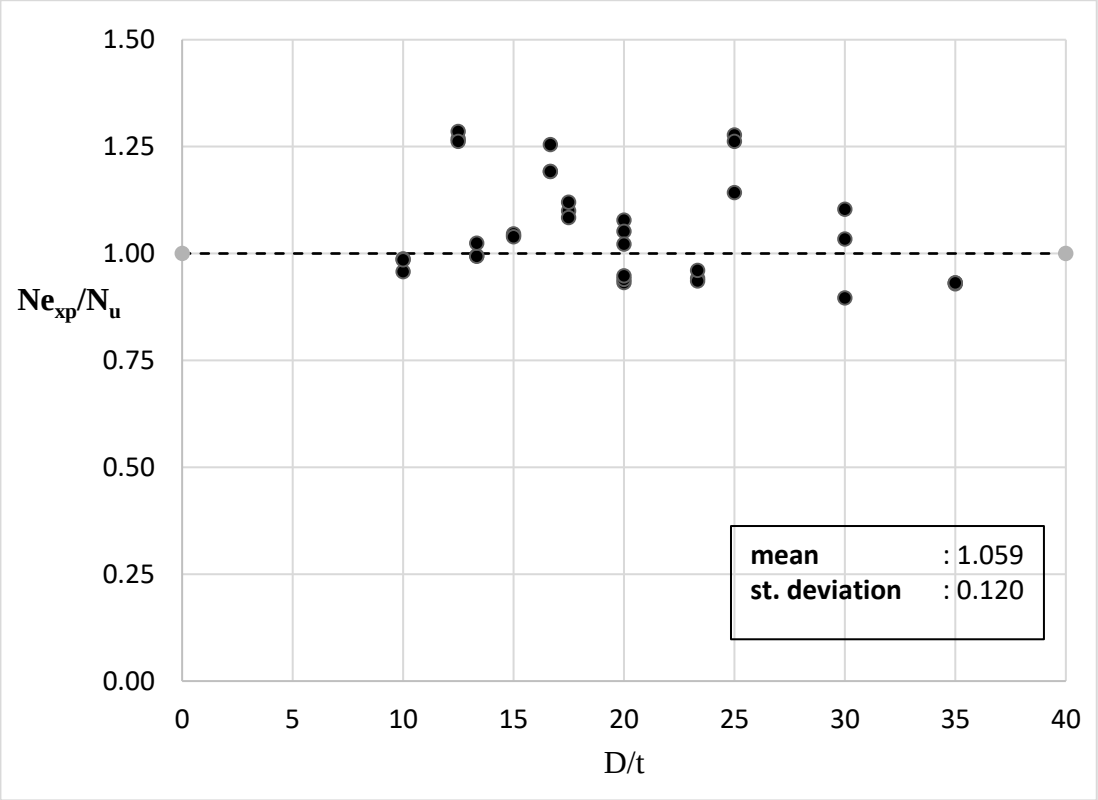

Figure 4.27 Comparisons between experimental and calculated values of PCFAT

As shown in Table 4.9 and Fig. 4.27, there is a good agreement between the experimental results and those obtained from the calculated results. This leads us to use these equations confidently in future PCFAT designs.

4.3.7.2 Model for the CFPFCAT tubes

The increase in load capacity due to the contribution of carbon fiber reinforced polymer (CFRP) confinement could be obtained by using the deformation-based increase index η_{cap} of the capacity by the following formula.

$$\eta_{cap} = \frac{N_{exp} - N}{N} \times 100\% \quad (4.12)$$

Here, *N* is the load of PCFAT at a deformation of axial shortening δ_u, N_{exp} is the load on CFPCFAT specimen at ultimate capacity as shown in Fig. 4.28. The calculated η_{cap} values are summarized in Table 4.10.

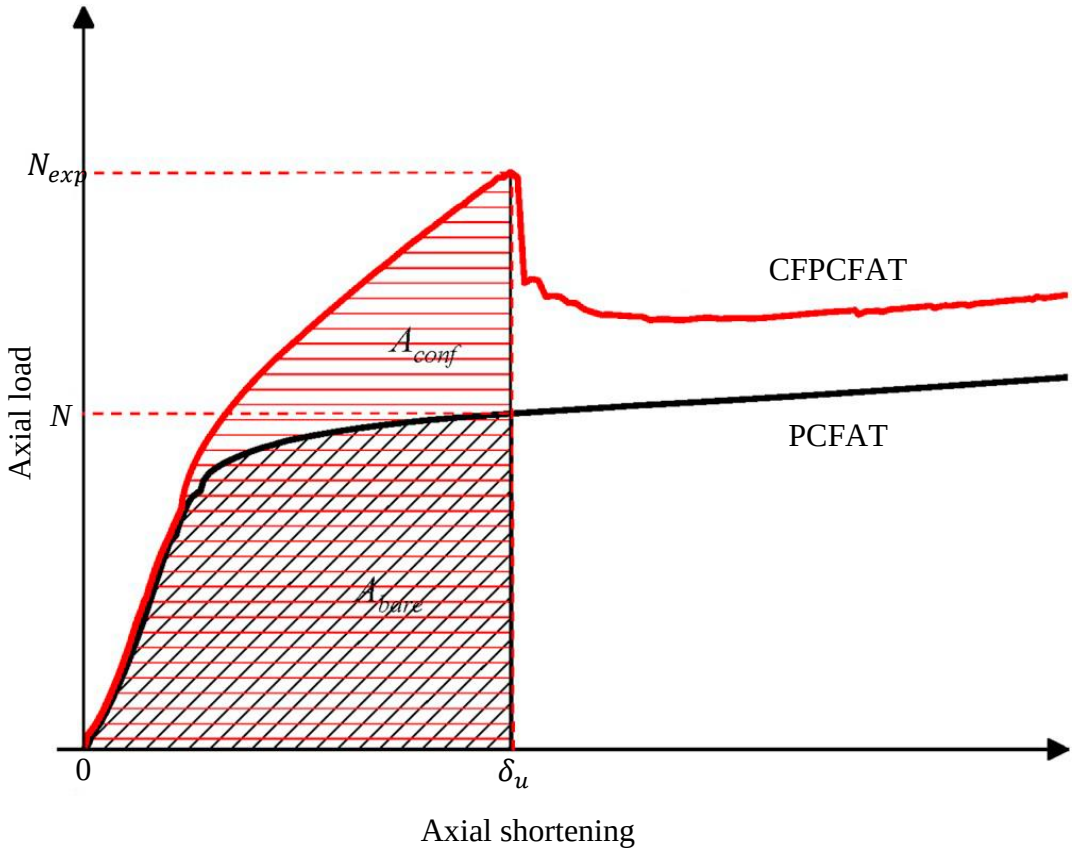

Figure 4.28 Increase index of capacity

In this study, the increase index also reflects the capacity of energy absorption of specimens. During the same shortening, the energy absorption of the CFPCFATs is higher than that for the PCFATs.

A confinement factor (ξ_{al}) used to describe the passive confinement of the aluminum tube on the polymer concrete core is defined as

$$\xi_{al} = \frac{A_{al}\sigma_{0.2}}{A_c f_{ck}} \tag{4.13}$$

where A_{al} is the cross-sectional area of aluminum tube, $\sigma_{0.2}$ is the 0.2% proof stress of aluminum obtained from the coupon tests. In addition, A_c is the cross-sectional area of polymer concrete core and f_{ck} is the characteristic strength of polymer concrete (=51.88 MPa).

The capacity increase index (η_{cap}) generally decreased with the increase in aluminum tube confinement factor ξ_{al}. However, with the same thickness of CFRP, the confinement effect of PCFATs reduce on the polymer concrete core when using a high thickness of the aluminum tube.

A confinement factor (ξ_{frp}) used to describe the passive confinement of the CFPCFAT tube on the polymer concrete core is

$$\xi_{frp} = \frac{A_{cf} f_{cf}}{A_c f_{ck}} \tag{4.14}$$

Here, A_{cf} is the cross-sectional area of CFRP sheet, f_{ck} is the tensile strength of CFRP sheet , which is 3500 MPa

The average load capacity enhancement percentage against confinement ratio (ξ_{frp}/ξ_{al}) is shown in Fig. 4.29.

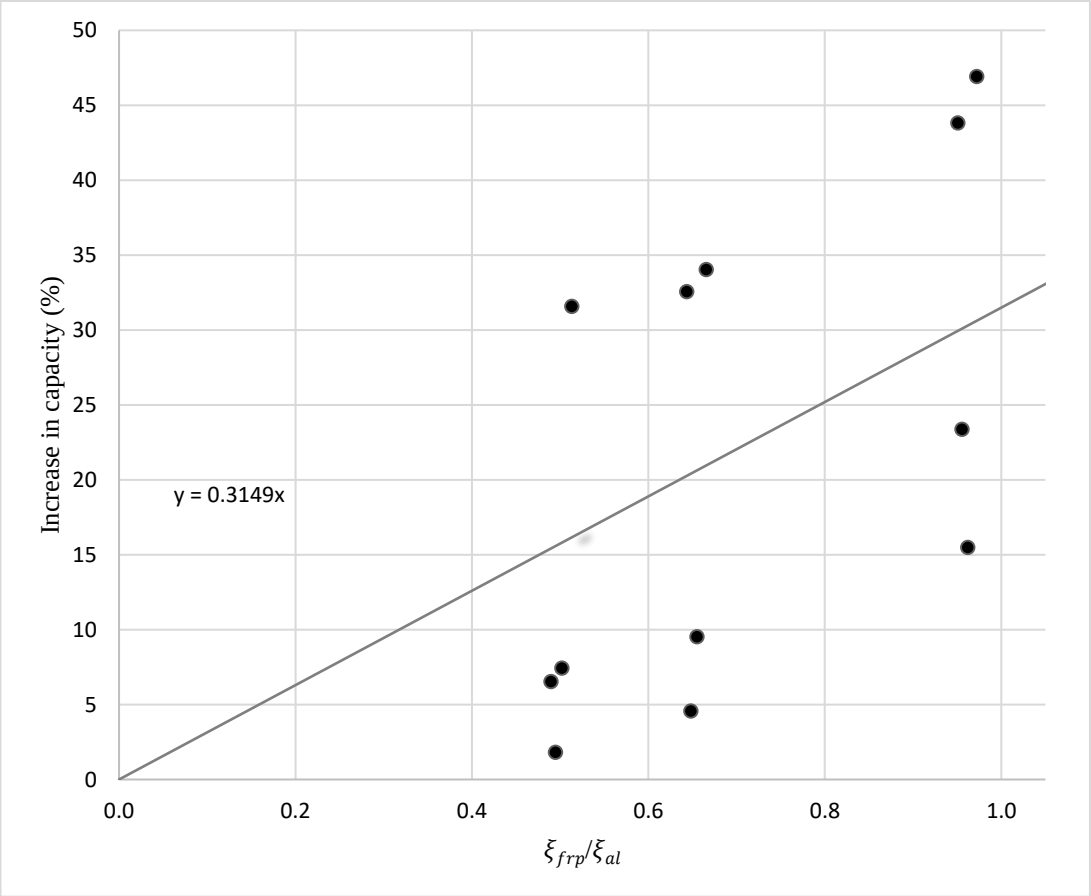

Figure 4.29 Increase in capacity versus ξ_{frp}/ξ_{al}

Fig. 4.29 shows that the average enhancement percentage in load-carrying capacity.In order to predict the axial load capacity of CFPCFAT specimens, a simplified method is used based on the trend line shown in Fig. 4.29, using the following equations:

$$N_u = (1 + \bar{\eta}_{cap})N_{PCFAT} \tag{4.15}$$

$$N_{PCFAT} = 1.27FA_{al} + 0.85f_c'A_c \tag{4.16}$$

$$\bar{\eta}_{cap} = 0.314\frac{\xi_{frp}}{\xi_{al}} \tag{4.17}$$

In the above equations, F is the minimum between the yield strength f_y and 70 % of ultimate tensile strength f_u of the aluminum tube, f_c' is the cylinder strength of polymer concrete, N_{PCFAT} stand for the load capacity of PCFAT tubes under axial compression as reported by AIJ [44], and $\bar{\eta}_{cap}$ is the capacity increase index obtained from the trend line in Fig. 4.29, which is 0.3149.

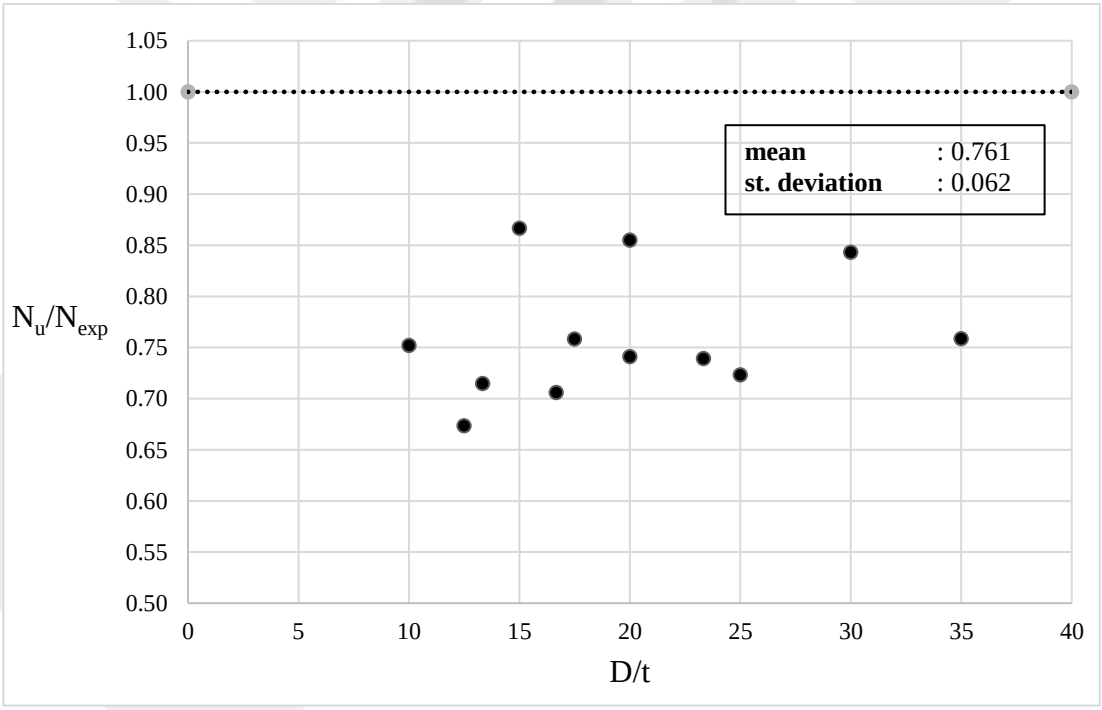

Figure 4.30 Comparison of the experimental and calculated results of CFPCFAT

Table 4.10 Calculated parameters and test results of CFPCFAT

Specimen	ξ_{al}	ξ_{frp}	ξ_{frp}/ξ_{al}	η_{cap} (%)	N_{PCFAT} (kN)	N_u (calculated) (kN)	Ultimate Load (N_{exp}) (kN)	N_u/N_{exp}
CFPCFAT120-2-1								
CFPCFAT120-2-2	1.105	1.074	0.972	46.915	103.990	135.826	183.299	0.741
CFPCFAT120-2-3								
CFPCFAT120-3-1								
CFPCFAT120-3-2	1.810	1.205	0.666	34.038	126.374	152.862	213.844	0.715
CFPCFAT120-3-3								
CFPCFAT120-4-1								
CFPCFAT120-4-2	2.650	1.360	0.513	31.575	147.478	171.306	227.808	0.752
CFPCFAT120-4-3								
CFPCFAT150-2-1								
CFPCFAT150-2-2	0.855	0.823	0.962	15.486	147.936	192.753	266.522	0.723
CFPCFAT150-2-3								
CFPCFAT150-3-1								
CFPCFAT150-3-2	1.373	0.899	0.655	9.529	176.714	213.164	302.004	0.706
CFPCFAT150-3-3								
CFPCFAT150-4-1								
CFPCFAT150-4-2	1.966	0.987	0.502	7.440	204.214	236.492	351.201	0.673
CFPCFAT150-4-3								
CFPCFAT180-2-1								
CFPCFAT180-2-2	0.697	0.666	0.955	23.376	198.805	258.617	306.795	0.843
CFPCFAT180-2-3								
CFPCFAT180-3-1								
CFPCFAT180-3-2	1.105	0.716	0.648	4.570	233.978	281.732	329.515	0.855
CFPCFAT180-3-3								
CFPCFAT180-4-1								
CFPCFAT180-4-2	1.561	0.772	0.495	1.807	267.873	309.608	357.309	0.866
CFPCFAT180-4-3								
CFPCFAT210-2-1								
CFPCFAT210-2-2	0.588	0.559	0.951	43.813	256.597	333.419	439.476	0.759
CFPCFAT210-2-3								
CFPCFAT210-3-1								
CFPCFAT210-3-2	0.925	0.595	0.643	32.548	298.166	358.565	485.190	0.739
CFPCFAT210-3-3								
CFPCFAT210-4-1								
CFPCFAT210-4-2	1.294	0.634	0.490	6.536	338.456	390.655	515.228	0.758
CFPCFAT210-4-3								

The calculated ultimate load capacity (N_u) were compared with the experimental values (N_{exp}) obtained in this study, as shown in Fig. 4.30 and Table 4.10. A mean ratio (N_u / N_{exp}) of 0.761 with a standard deviation of 0.062 was obtained. The model shows conservative results. The calculated results were generally lower than those of the experimental values, which leads us to believe that this model might not be suitable for this type of composite assemblies attributed to the different mechanical properties of used material, which will be led to different behaviour under the axial compression load. Moreover, in the model 2 and 3 layers for carbon fibers are used compared to 1 layer used in the present study. In addition, a variety of thicknesses and diameters are used in this research, while the model used only one diameter and that may definitely affect the efficiency of the model's accuracy when its used for this type of composite assemblies.

CHAPTER 5

CONCLUSION

5.1 Conclusions

In this research, the behaviour of polymer concrete-filled aluminum tubes (PCFAT) and carbon fiber reinforced polymer concrete filled aluminum tubes (CFPCFAT) under uniaxial compression load is investigated separately. A novel polymer concrete made of waste foundry sand (WFS) and rice husk ash (RHA) was used for filling the hollow aluminum tubes. In order to evaluate the strength of the composite tubes numerically, two design models were used. Based on the results, the following conclusions can be made:

- 96 % of the HCAT specimens failed by outward buckling around the circumference near the tube end, and 4 % failed by outward and inward buckling near the center. The failure mode depends on the diameter-to-thickness ratio. When this ratio increases, the failure mode will tend to outward and inward buckling, whereas the failure mode will tend to outward buckling only when the ratio decreases. The results also show the effect of the diameter-to-thickness ratio on the load-carrying capacity. When this ratio is increased, the specimens tend to have lower compressive strength.
- Using polymer concrete as infill significantly increases the load-carrying capacity and improves structural stability. However, the compressive strength decreases gradually with the increasing cross-sectional area of the assembly. The failure mode of PCFAT specimens was characterized by crushing stage of polymer concrete followed by local buckling of aluminum tube near the specimen's end. In addition, the aluminum tube thickness has a significant effect on this failure mode. When the thickness decreases, the failure mode becomes more pronounced.
- According to the test results, using carbon fiber reinforced polymer (CFRP) as additional reinforcement in CFPCFAT specimens shows improvement

in axial load capacity. The load-carrying capacity was increased up to 44 % compared to PCFAT. Carbon fiber reinforcement render the compressive strength values of PCFAT with various thickness values approach each other. CFPCFAT specimens generally failed by the rupture of the carbon fiber in the middle region of the sample due to the lateral expansion of the polymer concrete.

- The numerical model shows a good correlation with the experimental results for PCFAT specimens, with a mean ratio of 1.059 N_{exp} / N_u and a standard deviation of 0.120. In contrast, the calculated axial load capacities for CFPCFAT specimens show lower values than the experimental results with a mean ratio of 0.761 and standard deviation of 0.062 for $N_u / N_{exp.}$ This discrepancy is attributed to the different evolution of the material properties of hollow aluminum tubes with different dimensions during the extrusion process, even though the aluminum tubes have the same composition. Also, the geometric dimensions used in this study and in the utilized model are different.

5.2 Future studies

- There is still room to widen the range of PCFATs and CFPCFATs slenderness and breadth-to-thickness or diameter-to-thickness ratios in future research. In addition, more layers for the carbon fiber can be considered. This will expand the use of aluminum tube columns infilled with polymer concrete in structural applications.
- In addition to axial loading, future research on the behaviour of aluminum tubes filled with polymer concrete under cyclic and eccentric loading will enlarge the potential applications of these composite structural elements.
- Fire resistance of PCFATs is a common concern and must be carefully studied before using these tubes in practice. Future research is necessary to determine the behaviour of PCFAT columns under elevated temperatures.

REFERENCES

[1] J. Newman and B.S. Choo, *Advanced Concrete Technology Set*. U.K.: Butterworth-Heinemann, 2003, pp. 2-7.

[2] D.H. Koh, T.W. Kim, S.H. Jang, and H.W. Ryu, "Cancer Mortality and Incidence in Cement Industry Workers in Korea." *Safety and health at work*, vol. 2, pp. 243-249, Sep. 2011.

[3] P. Paulík, M. Bačuvčík, M. Brodňan, P. Koteš, and J. Vičan, "Reconstruction of the Oldest Reinforced Concrete Bridge in Slovakia in Krásno nad Kysucou." *Procedia Engineering*, vol. 156, pp. 334-339, Aug. 2016.

[4] L.H. Han, W. Li, and R. Bjorhovde, "Developments and advanced applications of concrete-filled steel tubular (CFST) structures: Members." *Journal of Constructional Steel Research*, vol. 100, pp. 211-228, Sep. 2014.

[5] J. Cho, J. Moon, H.J. Ko, and H.E. Lee, "Flexural strength evaluation of concrete-filled steel tube (CFST) composite girder." *Journal of Constructional Steel Research*, vol. 151, pp. 12-24, Dec. 2018.

[6] Y. Guo and Y. Zhang, "Comparative study of CFRP-confined CFST stub columns under axial compression." *Advances in Civil Engineering*, vol. 2018, Article ID 7109061, 8 pages, Jul. 2018.

[7] Y. Zhu, Y. Chen, K. He, R. Feng, X. Zhang, Q. Zhu, and C. Tang, "Flexural behavior of concrete-filled SHS and RHS aluminum alloy tubes strengthened with CFRP." *Composite Structures*, vol. 238, Article ID 111975, 23 pages, Apr. 2020.

[8] A. Aghi, "Investigation of waste foundry sand modified polymer concrete as a rapid repair material." M.S. thesis, Atilim University, Turkey, 2020.

[9] A.S. Momtazi, R.K. Khoshkbijar, and S.S. Mogharab, "Polymers in concrete: Applications and specifications." *European Online Journal of Natural and Social Sciences*, vol. 3, pp. 62–72, 2015.

[10] D.W. Fowler, “State of the art in concrete polymer materials in the US.” in *International Congress on Polymers in Concrete, Chuncheon, Korea*, 2007, pp. 29-36.

[11] A. Alganad, “Influence of waste foundry sand (WFS) and rice husk ash (RHA) on the mechanical properties of polymer concrete.” M.S. thesis, Atilim University, Turkey, 2020.

[12] C.S. Huang, Y.K. Yeh, G.Y. Liu, H.T. Hu, K.C. Tsai, Y.T. Weng, M.H. Wang, and M.H. Wu, “Axial load behavior of stiffened concrete-filled steel columns.” *Journal of Structural Engineering*, vol. 128(9), pp. 1222-1230, Sep. 2002.

[13] G. Giakoumelis and D. Lam, “Axial capacity of circular concrete-filled tube columns.” *Journal of Constructional Steel Research*, vol. 60(7), pp. 1049-1068, Jul. 2004.

[14] E. Ellobody, B. Young, and D. Lam, “Behaviour of normal and high strength concrete-filled compact steel tube circular stub columns.” *Journal of Constructional Steel Research*, vol. 62(7), pp. 706-715, Jul. 2006.

[15] P.K. Gupta, S.M. Sarda, and M.S. Kumar, “Experimental and computational study of concrete filled steel tubular columns under axial loads.” *Journal of Constructional Steel Research*, vol. 63(2), pp. 182-193, Feb. 2007.

[16] L.H. Han, W. Liu, and Y.F. Yang, “Behaviour of concrete-filled steel tubular stub columns subjected to axially local compression.” *Journal of Constructional Steel Research*, vol. 64(4), pp. 377-387, Apr. 2008.

[17] W.O. Oyawa, K. Sugiura, and E. Watanabe, “Polymer concrete-filled steel tubes under axial compression.” *Construction and Building Materials*, vol. 15(4), pp. 187-197, Jun. 2001.

[18] H. Tang, J. Chen, L. Fan, X. Sun, and C. Peng, “Experimental investigation of FRP-confined concrete-filled stainless steel tube stub columns under axial compression.” *Thin-Walled Structures*, vol. 146, Article ID 106483, 14 pages, Jan. 2020.

[19] F. Zhou and B. Young, “Tests of concrete-filled aluminum stub columns.” *Thin-Walled Structures*, vol. 46(6), pp. 573-583, Jun. 2008.

[20] F. Zhou and B. Young, " Concrete-filled aluminum circular hollow section column tests." *Thin-Walled Structures*, vol. 47(11), pp. 1272-1280, Nov. 2009.

[21] F. Zhou and B. Young, "Numerical analysis and design of concrete-filled aluminum circular hollow section columns." *Thin-walled Structures*, vol. 50(1), pp. 45-55, Jan. 2012.

[22] G. Nayak, K.K. Shetty, and S. Abdalla, " Effect of depth to thickness ratio and length to depth ratio on hollow section aluminum tubes filled with self-compacting concrete." *International Journal of Research in Engineering and Technology*, vol. 3(3), pp. 675-678, May. 2014.

[23] F.K. Idan, "Finite element analysis of concrete-filled aluminum tube columns." *International Journal of Applied Engineering Research*, vol. 12(12), pp. 3054-3062, 2017.

[24] F. Zhou and B. Young, "Concrete-filled double-skin aluminum circular hollow section stub columns." *Thin-Walled Structures*, vol. 133, pp. 141-152, Dec. 2018.

[25] E. Talebi, M. Korzen, A. Espinós, and S. Hothan, "The effect of damage location on the performance of seismically damaged concrete filled steel tube columns at fire." in *Proceedings of the 12th International Conference on Advances in Steel-Concrete Composite Structures, Spain*, 2018, pp. 835-842.

[26] M. Joni, C. Rexin, A. Mengesha, H.K. Kassa, C. Engineering, D. Tabor, and A. Region, "An experimental investigation on concrete filled aluminum tubular section retrofitted by using basalt strips." *International Research Journal of Engineering and Technology (IRJET)*, vol. 05(04), pp. 2270-2276, Apr. 2018.

[27] F.C. Wang, H.Y. Zhao, and L.H. Han, "Analytical behavior of concrete-filled aluminum tubular stub columns under axial compression." *Thin-Walled Structures*, vol. 140, pp. 21-30, Jul. 2019.

[28] V.I.L. Patel, Q.Q. Liang, and M.N. Hadi, "Numerical simulations of circular high strength concrete-filled aluminum tubular short columns incorporating new concrete confinement model." *Thin-Walled Structures*, vol. 147, Article ID 106492, 14 pages. Jan. 2020. https://doi.org/10.1016/j.tws.2019.106492

[29] ACI Committee 548, “Guide for the use of polymers in concrete.” U.S. ACI 548.1R-97, Sep. 24, 1997.

[30] ACI Committee 548, “Polymer concrete – Structural applications state-of-the-art report.” U.S. ACI 548.6R-96, Jan. 1, 1996.

[31] J.K. Fink, *Reactive Polymers: Fundamentals and Applications: A Concise Guide to Industrial Polymers*. William Andrew, 2017, pp. 1-45.

[32] B. Bhardwaj and P. Kumar. “Waste foundry sand in concrete: A review.” *Construction and Building Materials*, vol. 156, pp. 661-674, Dec. 2017.

[33] American Society for Testing and Materials, “Standard test methods for moisture, ash, and organic matter of peat and other organic soils.” U.S. ASTM D2974, Mar. 18, 2014.

[34] N.V. Tuan, G. Ye, K.V. Breugel, A.L.A. Fraaij and B.D. Dai, “The study of using rice husk ash to produce ultra-high-performance concrete.” *Construction and Building Materials*, vol. 25(4), pp. 2030–2035, Apr. 2011.

[35] A.C. Alfrey, “Aluminum,” in *Advances in Clinical Chemistry*, 1st ed., vol. 23. A.L. Latner Morton and Schwartz, Ed. New York: Academic Press, 1983, pp. 69–91.

[36] A.Ç. Kılınç, C. Durmuşkahya, and M.Ö. Seydibeyoğlu, “Natural fibers,” in *Fiber Technology for Fiber-Reinforced Composites*, 1st ed., M. Ozgur Seydibeyoglu, Amar Mohanty, and Manjusri Misra, Ed. Cambridge, England: Woodhead Publishing, 2017, pp. 209-235.

[37] F. Al-Mahmoud, “CFRP Reinforcement Rods,” in *Comprehensive Composite Materials II*, 2nd ed., vol. 3. Carl H. Zweben and Peter Beaumont, Ed. Amsterdam: Elsevier, 2017, pp. 578–591.

[38] European Committee for Standardization, “Tensile testing of metallic materials; method of test at ambient temperature.” Germany. DIN EN 10002-1, Apr. 1991.

[39] International Organization for Standardization, “Metallic materials - Sheet and strip - Determination of plastic strain ratio.” Switzerland. ISO 10113, May. 1991.

[40] American Society for Testing and Materials Standard, “Test method for compressive strength of cylindrical Concrete specimens.” U.S. ASTM C39, Apr. 1, 2015.

[41] European Committee for Standardization, “Testing hardened concrete. Compressive strength of test specimens.” Europ. EN, 12390-3, Apr. 8, 2002.

[42] J.W. Park, H.J. Yeom, and J.H. Yoo, “Axial loading tests and FEM analysis of slender square hollow section (SHS) stub columns strengthened with carbon fiber reinforced polymers.” *International Journal of Steel Structures*, vol. 13(4), pp. 731-743, Dec. 2013.

[43] K. Sakino, H. Nakahara, S. Morino, and I. Nishiyama, “ Behavior of centrally loaded concrete-filled steel-tube short columns.” *Journal of structural engineering*, vol. 130(2), pp. 180-188, Feb. 2004.

[44] Architectural Institute of Japan, “Recommendations for design and construction of concrete filled steel tubular structures.” Japan. 1997.